Scaling analysis of electron transport through metal-semiconducting carbon nanotube interfaces: Evolution from the molecular limit to the bulk limit

Yongqiang Xue*[1] and Mark A. Ratner[2]

[1] *College of Nanoscale Science and Engineering, University at Albany, State University of New York, Albany, New York 12203, USA**

[2] *Department of Chemistry and Materials Research Center, Northwestern University, Evanston, Illinois 60208, USA*

(Dated: March 22, 2022)

We present a scaling analysis of electronic and transport properties of metal-semiconducting carbon nanotube interfaces as a function of the nanotube length within the coherent transport regime, which takes fully into account atomic-scale electronic structure and three-dimensional electrostatics of the metal-nanotube interface using a real-space Green's function based self-consistent tight-binding theory. As the first example, we examine devices formed by attaching finite-size single-wall carbon nanotubes (SWNT) to both high- and low- work function metallic electrodes through the dangling bonds at the end, where the length of the SWNT molecule varies from the molecular limit to the bulk limit and the strength of metal-SWNT coupling varies from the strong coupling to the weak coupling limit. We analyze the nature of Schottky barrier formation at the metal-nanotube interface by examining the electrostatics, the band lineup and the conductance of the metal-SWNT molecule-metal junction as a function of the SWNT molecule length and metal-SWNT coupling strength. We show that the confined cylindrical geometry and the atomistic nature of electronic processes across the metal-SWNT interface leads to a different physical picture of band alignment from that of the planar metal-semiconductor interface. We analyze the temperature and length dependence of the conductance of the SWNT junctions, which shows a transition from tunneling- to thermal activation-dominated transport with increasing nanotube length. The temperature dependence of the conductance is much weaker than that of the planar metal-semiconductor interface due to the finite number of conduction channels within the SWNT junctions. We find that the current-voltage characteristics of the metal-SWNT molecule-metal junctions are sensitive to models of the potential response to the applied source/drain bias voltages. Our analysis applies in general to devices based on quasi-one-dimensional nanostructures including molecules, carbon nanotubes and semiconductor nanowires.

PACS numbers: 73.63.-b,73.40.-c,85.65.+h

I. INTRODUCTION

It is interesting to note that all the semiconductor devices that have had a sustaining impact on integrated microelectronics were invented before 1974,[1] the year when Chang, Esaki and Tsu reported the first observation of negative differential resistance (NDR) in semiconductor heterojunction resonant-tunneling diodes (RTD).[2] The operation of such semiconductor devices relies on the (controlled) presence of imperfections in otherwise perfect crystals,[3] through doping or through interfaces between materials with different electronic and/or lattice structures. Doping introduces electronic impurities (electrons/holes) into the otherwise perfect band structure through introducing atomic impuries (dopants) into the otherwise perfect lattice structure.[4] The presence of interfaces, on the other hand, induces spatial charge and potential inhomogeneities which control the injection and modulate the motion of excess charge carriers within the device. A number of fundamental buiding blocks of microelectronics can therefore be identified according to the interface structures that control the device operation,[1,5] including metal-semiconductor (MS) interfaces, semiconductor homo-(p-n) junctions, semiconductor heterojunctions and metal-insulator-semiconductor (MIS) interfaces.[1,5] Despite the continuous shrinking of feature size and correspondingly the increasing importance of hot-carrier and quantum mechanical effects,[6] the design and operation of semiconductor transistors have followed remarkably well the scaling rules for device miniaturization[7] derived from the semi-classical semiconductor transport equations.[8,9] There are also theoretical arguments that support the use of semiclassical pictures even in high-field transport[10] and nanoscale ballistic silicon transistors.[11]

The discovery of single-wall carbon nanotubes (SWNTs) in the early 1990s[12] has led to intense world-wide activity exploring their electrical properties and potential applications in nanoelectronic devices.[13,14,15] SWNTs are nanometer-diameter all-carbon cylinders with unique structure-property relations: They consist of a single graphene sheet wrapped up to form a tube and their physical properties are controlled by the boundary conditions imposed on the wrapping directions. They provide ideal artifical laboratories for studying transport on the length scale ranging from the molecular limit as all-carbon cylindrical molecules to the bulk limit as quasi-one-dimensional quantum wires with the same lattice configuration and local bonding environment.[13,14,15] Many device concepts well known in con-

ventional semiconductor microelectronics have been successfully demonstrated on a single-tube basis, ranging from intramolecular homo(hetero)-junctions, modulation doping to field-effect transitors.[16,17,18,19,20] This prompts interest in knowing if the physical mechanisms underlying the operation of conventional microelectronic devices remain valid down to such ultra-small scales. Research on SWNT-based nanoelectronic devices therefore presents unique opportunities both for exploring novel device technology functioning at the nano/molecular-scale and for re-examining the physical principles of semiconductor microelectronics from the bottom-up atomistic approach. In addition, the concepts and techniques developed can be readily generalized to investigate other quasi-one-dimensional nanostructures, in particular semiconductor nanowires.[21]

Among the device physics problems arising in this context, the nature of electron transport through a metal-semiconducting SWNT interface[22,23,24,26] stands out due to its simplicity and its role as one of the basic device building blocks.[1,5,27] As the device building block, it is also crucial for understanding the mechanisms and guiding the design of SWNT-based electrochemical sensors,[28] electromechanical devices,[29] and field-effect transistors (NTFET),[30,31,32] where electron transport through the metal-SWNT-metal junction is modulated through molecular adsorption, mechanical strain and electrostatic gate field respectively. Note that in the case of NTFET, metals have been used as the source, drain and gate electrodes, in contrast to silicon-based transistors which use heavily-doped polycrystalline materials.[30,31,32]

The nature of charge transport through metal-semiconductor interfaces has been actively investigated for decades due to their importance in microelectronic technology,[27,33,34] but is still not fully resolved, in particular regarding the mechanism of Schottky barrier formation/height and high-field transport phenomena.[35,36] Compared to their bulk semiconductor counterpart, metal-SWNT interfaces present new challenges in that: (1) Both the contact area and the active device region can have atomic-scale dimensions; (2) The quasi-one-dimensional structure (cylindrical for nanotube materials) makes the screening of electron-electron interaction ineffective and leads to long range correlation between electrons within SWNT-based devices; (3) Last but probably the most important difference lies in the fact that quasi-one-dimensional wires, no matter how long, cannot be treated as electron reservoirs.[37] This is partly due to the fact that the restricted phase space in such systems prevents rapid relaxation of injected carriers to a pre-defined equilibrium state through electron-electron and/or electron-phonon scatterings. But more importantly, this can be understood from a simple geometrical argument: Since the total current is conserved, there will always be a finite current density flowing along the wire and consequently a non-equilibrium state persists no matter how strong electron-electron and/or electron-phonon scattering is. An equilibrium state can be achieved only through the widened (adiabatic) contact with the (three-dimensional) metallic electrodes (or other macroscopic measurement apparatus) attached to them, where the finite current density can be effectively "diluted" through the larger cross sectional area.[37] *Correspondingly electron transport through metal-SWNT interfaces can only be studied within the configuration of metal-SWNT-metal junction* (as are other quasi-one-dimensional systems), in contrast to the planar metal-semiconductor interface, where the presence of the second electrode can be implicitly neglected and the analysis of transport characteristics proceeds by analyzing the interface region and the bulk semiconductor region separately.[27]

The last fact has important implications in the assessment of Schottky barrier effects on the measured transport characteristics, since transport mechanisms both at the interface and inside the active device region have to be considered simultaneously even for a long nanotube. Since the back-scattering of electrons by impurities[38] and the low-energy acoustic phonons[39,40,41] are weak in such quasi-one-dimensional systems, the nature of the electron transport through metal-SWNT interfaces generally depends on the type of the SWNTs (length/diameter/chirality), the type of the contacts, and the temperature and bias voltage range. Experimentally, this matter is further complicated by the different fabrication/contact schemes used and the lack of knowledge of the atomic structure of the SWNT junctions.

Recent works have studied electrical transport through a metal-long carbon nanotube interface using the bulk (infinitely long) band structures and electrostatics of ideal cylinders[23,24,25,26]. For nanoelectronics research, it will be important to explore the device functionality of finite-size carbon nanotubes with lengths ranging from nanometers to tens of nanometers. Since most of the SWNT devices currently investigated are based on SWNTs with length of $100nm$ or longer, an investigation of the finite-size effect will shed light on the scaling limit of carbon nanotube devices,[42,43,44] as well as establish the validity or viability of using bulk device physics concepts in nanotube device research.

The finite-size SWNT can be either a finite cylindrical all-carbon molecule attached to the metal surfaces through the dangling bonds at the end (end-contact scheme),[45] a finite segment of a long carbon nanotube wire whose ends are buried inside the metallic electrodes (embedded-contact scheme),[19,46] or a finite segment of a long nanotube wire which is deposited on top of predefined metallic electrodes and side-contacted to the surfaces of the electrodes (side-contact sheme).[13,47] In the case of finite SWNT molecules, a transition from the molecular limit to the bulk (infinitely long) limit in the electronic structure will occur as the length of the finite SWNT varies from nanometers to tens of nanometers. In the case of long SWNT wires, the electronic structure of the finite SWNT segment remains that of the bulk (which may be perturbed by the coupling to the electrodes), but the electrostatics of the metal-SWNT-metal junction varies with the SWNT length. Due to the nanoscale contact geometry and reduced dimensionality of

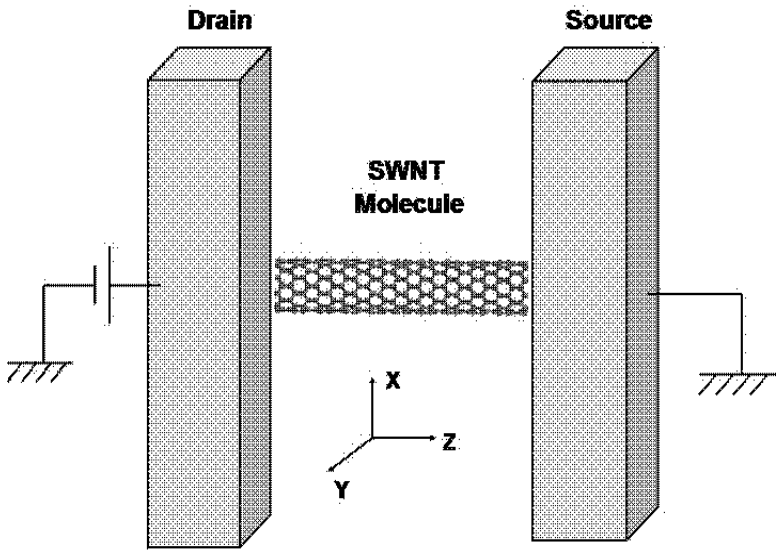

FIG. 1: (Color online) Schematic illustration of the metal-SWNT molecule-metal junction. We have also shown the coordinate system of the SWNT junction.

SWNTs, a correct description of the Schottky barrier formation at the metal-finite SWNT interface generally requires an atomistic description of the electronic processes throughout the metal-SWNT-metal junctions.

The purpose of this work is thus to present a self-consistent atomistic analysis of the electronic and transport properties of the metal-SWNT interfaces within the configuration of metal-SWNT-metal junction as a function of the SWNT length, which is varied from the nanometer to tens of nanometer range. In contrast to previous theoretical works,[22,23,24,25,26] we use a novel Green's function based self-consistent tight-binding (SCTB) theory in real-space, which takes fully into account the three-dimensional electrostatics and the atomic-scale electronic structure of the SWNT junctions. In accordance with the nanometer length-scale of the SWNT studied, we treat electron transport within the coherent transport regime.[40,41] In this first paper, we consider the device formed by attaching a finite cylindrical SWNT molecule to the electrode surface through the dangling bonds at the end (Fig. 1). The case of a finite-segment of long SWNT wires in both embedded-contact and side-contact schemes will be treated in the subsequent paper.

The device configuration considered here represents an atomic-scale analogue (both the contact area and the active device region are atomic-scale) to the planar metal-semiconductor interface, where dangling bonds also exist at the semiconductor surface layers and contribute to the Schottky barrier formation.[33,34] Compared to other molecular-scale devices where the individual organic molecule is self-assembled onto the metallic electrode through appropriate end groups[48,49,50], the SWNT molecule presents a homogeneous device structure where the only electronic inhomogeneity is introduced at the metal-SWNT interface through the ring of dangling-bond carbon atoms. The device structure considered here thus provides an ideal system for studying the length dependence of device characteristics on an atomic scale. In particular, the effect of the coupling strength can be studied by varing the SWNT end-electrode surface distance.

The rest of the paper is organized as follows: We present the details of the Green's function based self-consistent tight-binding model in section II. We analyze the evolution of the SWNT electronic structure with the length of the SWNT molecules in section III. We devote section IV to analyzing the nature of Schottky barrier formation at the metal-SWNT molecule interface by examining the electrostatics (change transfer and electrostatic potential change), the electron transmission characteristics and the "band" lineup. In section V, we present the temperature and length dependence of the SWNT junction conductance. We show in section VI that the current-voltage (I-V) characteristics of the SWNT junction are sensitive to the spatial variation of the voltage drop across the junction. Finally in section VII, we summarize our results and discuss their implications for the functioning of SWNT-based devices. A preliminary report of some of the results presented here has been published elsewhere.[45] We use atomic units throughout the paper unless otherwise noted.

II. THEORETICAL MODEL

A. Real-space Green's function based self-consistent tight-binding (SCTB) theory

Modeling electron transport in nanoscale devices is much more difficult than in bulk and mesoscopic semiconductor devices due to the necessity of including microscopic treatment of the electronic structure and the contacts to the measurement electrodes, which requires combining the non-equilibrium statistical mechanics of a open quantum system[51,52,53] with an atomistic modeling of the electronic structure.[54,55]. For small molecular-scale devices where the inelastic carrier scattering can be neglected, this has been done using a self-consistent Matrix Green's function (SCMGF) method,[49,50,54] which combines the Non-Equilibrium Green's Function (NEGF) theory of quantum transport[56,57] with an effective single-particle description of the electronic structure using density-functional theory (DFT).[58] To treat larger nanoscale systems, e.g., carbon nanotubes or semiconductor nanowires containing thousands or tens of thousands of atoms, a simpler tight-binding-type theory is more appropriate.[59,60,61,62,63,64,65] Correspondingly, we have developed a real-space self-consistent tight-binding (SCTB) method which includes atomic-scale description of the electronic structure and the three-dimensional electrostatics of the metal-SWNT-metal junction. The method is essentially the semi-empirical version of the SCMGF method for treating molecular electronic devices and is applicable to arbitrary nanostructured devices. The details and applications of the SCMGF method have been described extensively elsewhere[49,50,54], here we give a brief summary of the self-consistent tight-binding implementation.

The method starts from the Hamiltonian H_0 describing the isolated nanostructure and the bare metallic electrodes, which can be obtained using either *ab initio* or empirical approaches as appropriate. The effect of the coupling to the electrodes is included as self-energy operators.[56,57] The coupling to the external contacts leads to charge transfer between the electrodes and the nanostructure. Applying a finite bias voltage also leads to charge redistribution (screening) within the nanostructure. Both the effect of the coupling to the contact and the screening of the applied field thus introduced will need to be treated self-consistently. The Hamiltonian describing the coupled metal-nanostructure-metal junction is thus $H = H_0 + V_{ext} + \delta V[\delta\rho]$, where an external potential of the type $V_{ext}(\vec{r}) = -e\vec{E}\cdot\vec{r}$ should be added in the case of a nonzero source-drain or gate voltage and $\delta\rho$ is the change in the charge density distribution. Given the Hamiltonian matrix, the density matrix ρ_{ij} and therefore the electron density are calculated using the Non-Equilibrium Green's Function (NEGF) method[54,55,56,57] from either

$$G^r = \{E^+S - H - \Sigma_L(E) - \Sigma_R(E)\}^{-1}, \tag{1}$$

$$\rho = \int \frac{dE}{2\pi} Imag[G^r](E). \tag{2}$$

for device at equilibrium or

$$\begin{aligned} G^< &= i[G^r(E)\Gamma_L(E)G^a(E)]f(E-\mu_L) \\ &+ i[G^r(E)\Gamma_R(E)G^a(E)]f(E-\mu_R), \end{aligned} \tag{3}$$

$$\rho = \int \frac{dE}{2\pi i} G^<(E). \tag{4}$$

for device at non-equilibrium. Here S is overlap matrix and $f(E-\mu_{L(R)})$ is the Fermi-Dirac distribution function at the left (right) electrode. The Green's functions G^r and $G^<$ are defined in the standard manner.[56,57] $\Sigma_{L(R)}$ is the self-energy operator due to the coupling to the left (right) electrode which is calculated from the metal surface Green's function, while $\Gamma_{L(R)} = i(\Sigma_{L(R)} - (\Sigma^\dagger_{L(R)})$ (See Refs. 54,56 for details).

Within the local-density-approximation of density-functional theory,[58] the long range part of δV is just the coulomb potential $\delta V(\vec{r}) = \int \frac{\delta\rho(\vec{r}')}{|\vec{r}-\vec{r}'|} d\vec{r}'$. For self-consistent treatment of the charging effect within the tight-binding formulation, we follow the density-functional tight-binding (DFTB) theory developed by Frauenheim and coworkers[65] by approximating the charge distribution as a superposition of normalized atomic-centered charge distributions $\delta\rho(\vec{r}) = \sum_i \delta N_i \rho_i(\vec{r}-\vec{r}_i)$ where δN_i is the net number of electrons on atomic-site i and ρ_i is taken as a normalized Slater-type function $\rho_i(\vec{r}) = \frac{1}{N_{\zeta_i}} e^{-\zeta_i r}$ and $\int d\vec{r}\rho_i(\vec{r}) = 1$. The exponent ζ_i is chosen such that the electron-electron repulsion energy due to two such charge distributions on atomic-site i equals the difference between the atomic electronic affinity and ionization potential $\int d\vec{r}d\vec{r}'\rho_i(\vec{r})\rho_i(\vec{r}')/|\vec{r}-\vec{r}'| = I_i - A_i$[65], which incorporates implicitly the short-range on-site electron-electron interaction effect. In this way, the change in the electrostatic potential can be written as superposition of atomic-centered potentials $\delta V(\vec{r}) = \sum_i \delta N_i V_i(\vec{r}-\vec{r}_i)$. The advantage of the present approximation is that $V_i(\vec{r}-\vec{r}_i) = \int d\vec{r}'\rho_i(\vec{r}'-\vec{r}_i)/|\vec{r}-\vec{r}'|$ can be evaluated analytically,[65,66]

$$V_i = (1 - e^{-\zeta_i|\vec{r}-\vec{r}_i|}(1 + \zeta_i|\vec{r}-\vec{r}_i|/2))/|\vec{r}-\vec{r}_i|. \tag{5}$$

For the metal-SWNT-metal junction considered here, we take into account the image-potential effect by including within δV contributions from both atom-centered charges and their image charges (centered around the image positions), rather than imposing an image-type potential correction on δV. The charge transfer-induced electrostatic potential change is thus:

$$\delta V(\vec{r}) = \sum_i [\delta N_i V_i(\vec{r} - \vec{r}_i) + \delta N_{i;image} V_i(\vec{r} - \vec{r}_{i;image})] \tag{6}$$

where the image charges $\delta N_{i;image}$ and their positions $\vec{r}_{i;image}$ are determined from standard electrostatics considerations.[67,68] The self-consistent cycle proceeds by evaluating the matrix elements of the potential $\delta V_{mn} = \int d\vec{r}\phi^*_m(\vec{r})\delta V(\vec{r})\phi_n(\vec{r})$ using two types of scheme: (1) If m, n belong to the same atomic site i, we calculate it by direct numerical integration; (2) If m, n belong to different atomic sites, we calculate it from the corresponding on-site element using the approximation $\delta V_{mn} = 1/2 S_{mn}(\delta V_{mm} + \delta V_{nn})$ where S_{mn} is the corresponding overlap matrix element. We also calculate the matrix elements of the external potential V_{ext} by direct numerical integration whenever applicable. Given the Hamiltonian matrix $H = H_0 + V_{ext} + \delta V$, the self-consistent calulation then proceeds by calculating the density matrix ρ from the Green's function by integrating over a complex energy contour[49,50,54,69] and evaluating the net charge on atomic-site i from $\delta N_i = (\rho S)_{ii} - N_i^0$ where N_i^0 is the number of valence electrons on atomic-site i of the bare SWNT. Note that the advantage of the present self-consistent tight-binding treatment is that *no adjustable parameters have been introduced* besides those that may be present in the initial Hamiltonian H_0.

Once the self-consistent calculation converges, we can calculate the transmission coefficient through the SWNT junction from

$$T(E, V) = Tr[\Gamma_L(E, V) G^r(E, V) \Gamma_R(E, V) [G^r]^\dagger(E, V)], \tag{7}$$

and the spatially-resolved local density of states (LDOS) from

$$n(\vec{r}, E) = -\frac{1}{\pi} \lim_{\delta \to 0^+} \sum_{ij} Imag[G^r_{ij}(E + i\delta)] \phi_i(\vec{r}) \phi^*_j(\vec{r}), \tag{8}$$

The spatial integration of LDOS gives the density of states,

$$n^\sigma(E) = \int d\vec{r} n^\sigma(\vec{r}, E) = -\frac{1}{\pi} \lim_{\delta \to 0^+} Tr\{Imag[G^r(E + i\delta)]S\} = \sum_i n_i(E) \tag{9}$$

where the atomic site-resolved density of states is $n_i(E) = -\frac{1}{\pi} \lim_{\delta \to 0^+} [Imag[G^r(E + i\delta)]S]_{ii}$. Within the coherent transport regime, the terminal current is related to the transmission coefficient through the Landauer formula[51,52,53]

$$I = \frac{2e}{h} \int dE T(E, V)[f(E - \mu_L) - f(E - \mu_R)] \tag{10}$$

where we can separate the current into two components, the "tunneling" component I_{tun} and the "thermionic emission" component I_{th} as follows,

$$I = I_{tun} + I_{th} = \frac{e}{h}[\int_{\mu_L}^{\mu_R} + (\int_{-\infty}^{\mu_L} + \int_{\mu_R}^{+\infty})] dE T(E, V)[f(E - \mu_L) - f(E - \mu_R)] \tag{11}$$

Similarly, we can separate the zero-bias conductance

$$G = \frac{2e^2}{h} \int dE T(E)[-\frac{df}{dE}(E - E_F)] = G_{Tu} + G_{Th} \tag{12}$$

into the tunneling contribution $G_{tun} = \frac{2e^2}{h} T(E_F)$ and thermal-activation contribution $G_{th} = G - G_{tun}$.

B. Device model

In this work, we take $(10, 0)$ SWNT as the protype semiconducting SWNT. Since for metal-semiconductor contacts, high- and low- work function metals are used for electron injection and hole-injection respectively, we consider both gold (Au) and titanium (Ti) electrodes as examples of high- and low- work function metals (with work functions of 5.1 and 4.33 eV respectively[70,71]). The work function of the (10,0) SWNT is taken the same as that of the graphite

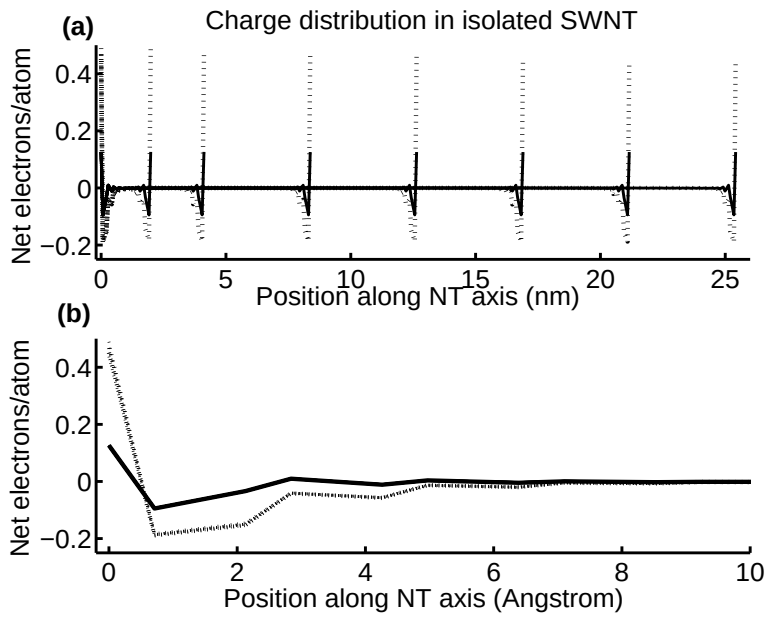

FIG. 2: (a) shows net electron distribution in the isolated SWNT molecule as a function of SWNT length for seven different lengths. (b) shows magnified view at the left end of all SWNT molecules studied. Here the solid lines show the results obtained using EHT with self-consistent correction, while the dotted lines show the results obtained using EHT without self-consistent correction.

(4.5 eV)[16,17]. In this paper, the Hamiltonian H_0 describing the bare SWNT is obtained using the semi-empirical Extended Huckel Theory (EHT) with corresponding non-orthogonal Slater-type basis sets $\phi_m(\vec{r})$[72,73] describing the valence (sp) electrons of carbon, while the self-energy due to the contact to the metallic electrodes is evaluated using tight-binding parameters obtained from fitting accurate bulk band structure.[54,74] The calculation is performed at room temperature.

The $(10,0)$ SWNT has a diameter of $7.8(\mathring{A})$ and unit cell length of $4.1(\mathring{A})$. The unit cell consists of 4 carbon rings with 10 carbon atoms each. The calculated bulk band gap using EHT is $\approx 0.9(eV)$. Since the contacts involved in most transport measurement are not well characterized, a microscopic study as presented here necessarily requires a simplified model of the interface, which is illustrated schematically in Fig. 1. Here the finite SWNT molecules are attached to the electrode surface through the ring of dangling-bond carbon atoms at the ends. We neglect the possible distortion of the SWNT atomic structure induced by the open-end and its subsequent adsorption onto the electrode surface.[47] We assume that the axis of the SWNT molecule (the Z-axis) lies perpendicular to the electrode surface (the XY-plane). Only nearest-neighbor metal atoms on the surface layer of the electrode are coupled to the SWNT end, the surface Green's functions of which are calculated using the tight-binding parameter of Ref. 74 assuming a semi-inifinte substrate corresponding to the $\langle 111 \rangle$ and hcp surface for the gold and titanium electrodes respectively.

The lengths of the $(10,0)$ SWNT molecule investigated are $L = 2.0, 4.1, 8.4, 12.6, 16.9, 21.2$ and 25.4 (nm), corresponding to $5, 10, 20, 30, 40, 50$ and 60 unit cells respectively. As discussed in the following sections, the variation of SWNT length from 5 to 60 unit cells spans the entire range from the molecular limit to the bulk limit. To evaluate the dependence of Schottky barrier formation on the strength of metal-SWNT interface coupling, we consider three SWNT end-metal surface distances of $\Delta L = 2.0, 2.5$ and $3.0(\mathring{A})$. Note that the average of the nearest-neighbor atom distance in the SWNT and Au/Ti electrode is around $2.1(\mathring{A})$. From our previous work on first-principles based modeling of molecular electronic devices,[50] we find that increasing metal-molecule distance by $1.0(\mathring{A})$ is sufficient to reach the weak interfacial coupling limit. Therefore the three choices of metal-SWNT distance are sufficient to demonstrate the trend of Schottky barrier formation as the strength of interface coupling varies from the strong coupling to the weak coupling limit.

III. EVOLUTION OF THE ELECTRONIC STRUCTURE OF THE SWNT MOLECULE WITH LENGTH

The dangling σ bonds at the open end of the SWNT molecule lead to charge transfer between carbon atoms at the end and carbon atoms in the interior of the SWNT. This should be corrected self-consistently first and gives

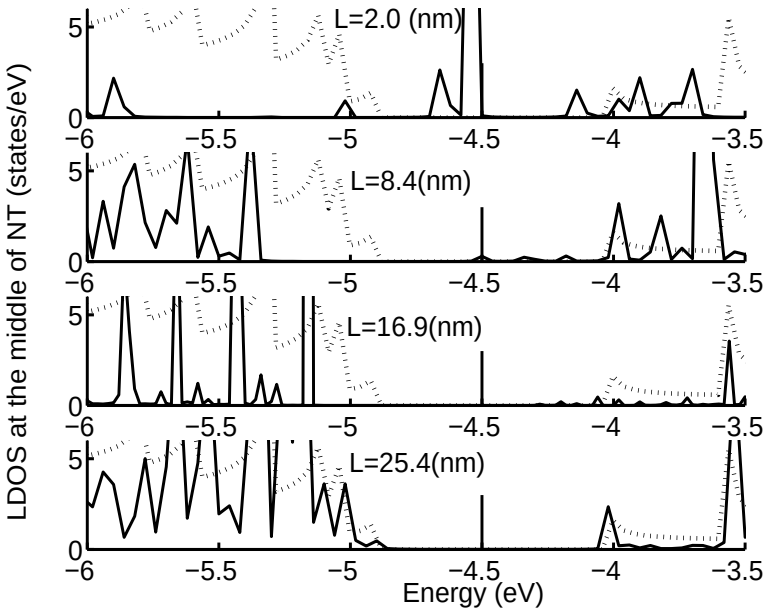

FIG. 3: Local density of states in the middle of the $(10,0)$ SWNT molecule calculated using the self-consistent EHT for SWNT lengths of $2.0, 8.4, 16.9$ and $25.4(nm)$ respectively. The vertical line at $E = -4.5(eV)$ denotes the Fermi-level position of the bulk SWNT. The dotted line is the LDOS of the bulk $(10,0)$ SWNT. For clarity, the figures have been cut off at the top where necessary.

the intial charge configuration $N_i^0$for determining the charge transfer within the metal-SWNT-metal junction in later sections. The self-consistent calculation proceeds as described in the previous section, except that there is no self-energy operator associated with the contact in the case of the bare SWNT molecule. The result is shown in Fig. 2, where we plot the net electrons per atom as a function of position along the $(10,0)$ SWNT axis obtained from both EHT and the self-consistent EHT calculations. The self-consistent treatment suppresses both the magnitude and the range of the charge transfer, which are approximately the same for all the SWNT molecules investigated, reflecting the localized nature of the perturbation induced by the end dangling bonds (Fig 2(b)).

To evaluate the evolution of SWNT electronic structure with molecule length, we calculated the local density of states in the middle unit cell of the SWNT molecule using the self-consistent EHT and compared them with those of the bulk (infinitely long) SWNT. The results for SWNT lengths of $2.0, 8.4, 16.9$ and $25.4(nm)$ are shown in Fig. 3. Here the LDOS of the isolated finite SWNT molecule is artificially broadened by inserting a small but finite imaginary number ($\delta = 10^{-6}(eV)$) into the retarded Green's function $G^r(E + i\delta)$. Therefore only the band edge location but not the exact value of the LDOS should be examined when evaluating the approach to the bulk limit with increasing nanotube length. The LDOS of the shortest SWNT molecule (2.0 nm) shows completely different structure from that of the bulk. In particular, there are peaks located within the conduction-valence band gap of the bulk SWNT caused by the localized dangling bond states at the end, which decays into the interior of the short SWNT molecule. This is illustrated by the position-dependent LDOS along the NT axis in Fig. 4. We can therefore characterize the 5-unit cell SWNT as being in the molecular limit. The magnitude of the localized dangling-bond states in the middle is suppressed exponentially with increasing SWNT length and is negligible for all other SWNT molecules studied.

The development of the SWNT valence bands with molecule length is clear from Fig. 3. The development of the SWNT conduction bands is less regular since tight-binding theory constructed for valence electrons generally describes the valence bands better than the conduction bands.[75] The approach to the bulk band structure is obvious for SWNT longer than 40 unit cells and complete for the SWNT molecules of 60 unit cells long. Therefore the variation of SWNT length from 5 to 60 unit cells spans the entire range from the molecular limit to the bulk limit. Note that as the length of the SWNT molecule changes, the energy of localized dangling bond states also changes, which saturates as the SWNT approaches the bulk limit. For the 60-unit cell SWNT, it is located around $-4.5(eV)$, i.e., the Fermi-level of the bulk SWNT. This is consistent with the previous observation in semiconductor interfaces, where it has been argued that the dangling bond level plays the role of "charge-neutrality-level" (CNL) in band lineup involving semiconductors, which is located around the midgap for semiconductors with approximately symmetric conduction and valence band structures.[76,77]

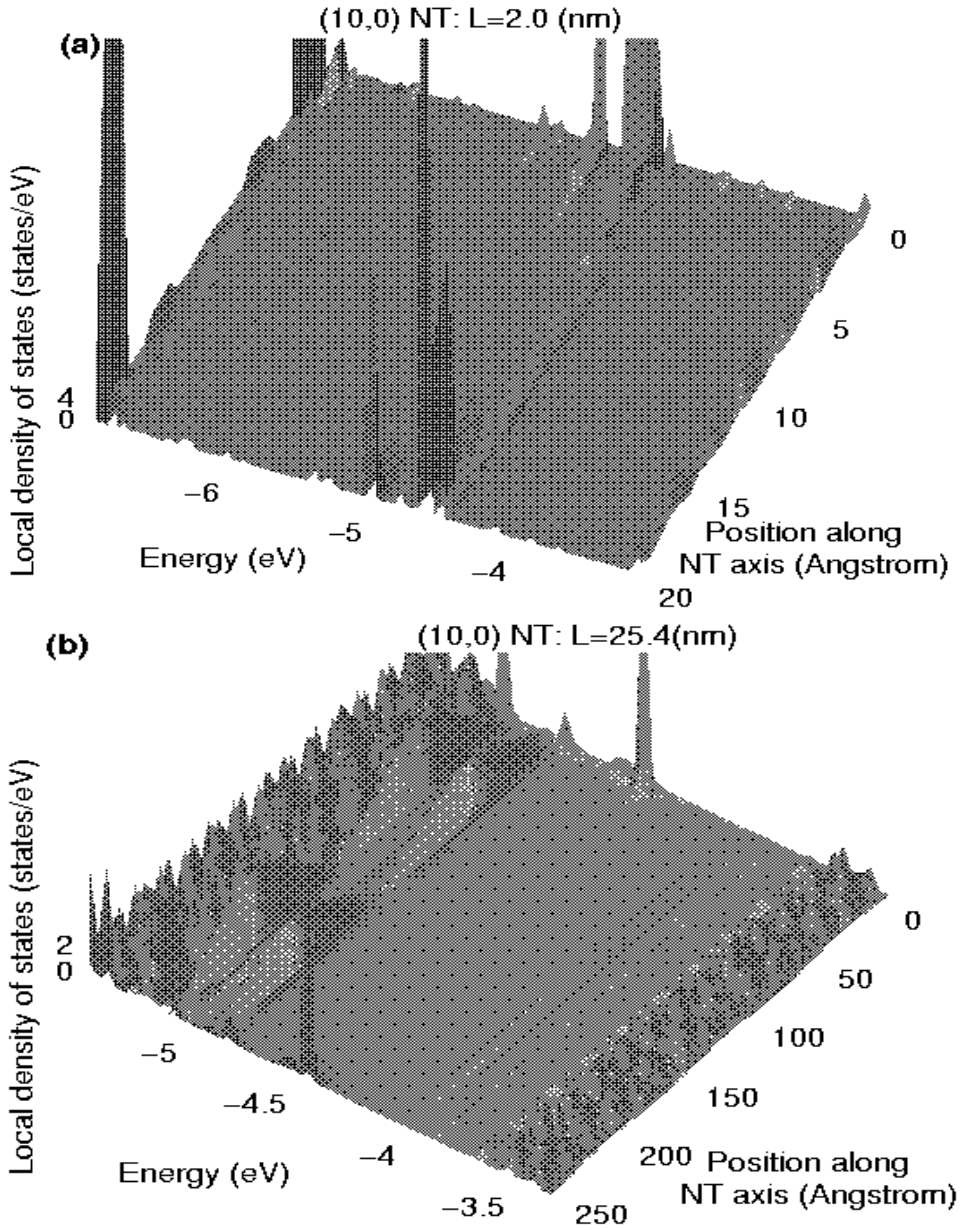

FIG. 4: (Color online) Local density of states as a function of position along the axis of the 5-unit cell (a) and 60-unit cell (b) SWNT molecule. The LDOS is obtained by summing over the 10 carbon atoms of each ring of the $(10, 0)$ SWNT. Each cut along the energy axis for a given position along the NT axis gives the LDOS at the corresponding carbon ring. Each cut along the postion axis for a given energy illustrates the spatial extension of the corresponding electron state. For the 5-unit cell SWNT(a), localized dangling bond state exists around $-5.0(eV)$, whose wavefunction decays into the interior of the SWNT molecule. For the 60-unit cell SWNT which has approached the bulk limit, the localized dangling bond state is located instead around $-4.5(eV)$, .i.e., the middle of the conduction/valence band gap.

IV. SCALING ANALYSIS OF SCHOTTKY BARRIER FORMATION AT METAL-SWNT MOLECULE INTERFACES

A. Schottky barrier formation at planar metal-semiconductor interfaces

We start with a brief summary of Schottky barrier formation at an ideal planar metal-semiconductor interface[33,34,77] to motivate our discussion of metal-SWNT interface in later sections. An ideal metal-semiconductor interface is formed by reducing the distance between a metal and a semi-infinite semiconductor until an intimate and abrupt interface

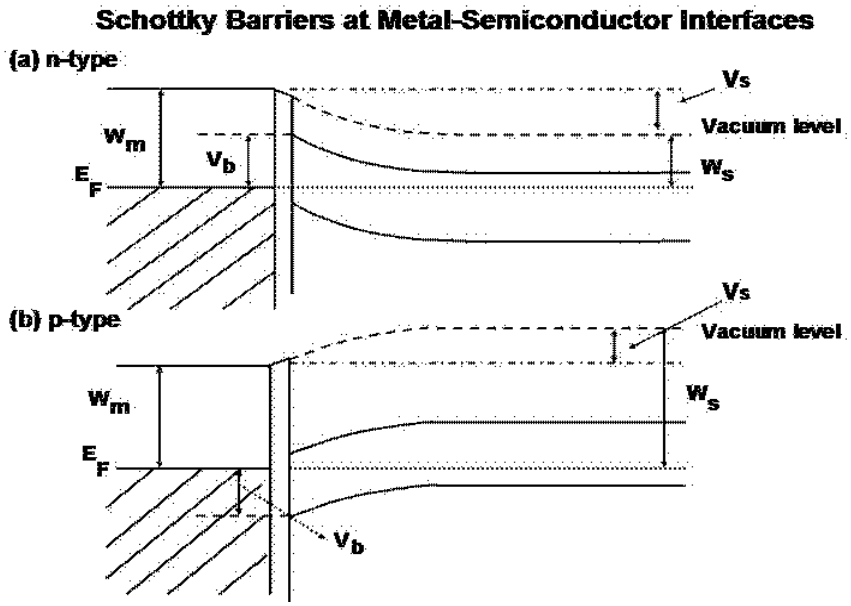

FIG. 5: Schematic illustration of the formation of Schottky barrier at the planar metal-semiconductor interfaces. (a) n-type semiconductor; (b) p-type semiconductor. W_m, W_s are the work functions of the metal and semiconductor respectively. V_b is the Schottky barrier height for electron (hole) injection at the n-type (p-type) semiconductor interface. V_s is the additional potential shift inside the semiconductor due to the depleted dopant charges.

forms,[33] as illustrated in Fig. 5.

The open-end of the semi-infinite semiconductor leads to localized surface states whose wavefunctions decay exponentially into the vacuum and inside the semiconductor, the nature of which can be undersood qualitatively from the complex band structure of the bulk semiconductor by extrapolating the energy band into the band gap region. Upon contact with the metal electrodes, the intrinsic semiconductor surface states are replaced by Metal-Induced Gap States (MIGS), which are the tails of the metal wavefunction decaying into the semiconductor within the band gap since the wavefunctions there are now matched to the continuum of states around the metal Fermi-level.[79,80] The corresponding charge transfer induces an interface dipole layer due to the planar structure, the electrostatic potential drop across which shifts rigidly the semiconductor band relative to the metal Fermi-level E_F. Additional electrostatic potential change can also occur if the semiconductor is doped and a space-charge layer forms due to the depleted dopant charges, as illustrated in Fig. 5. The total potential shift must be such that the two Fermi-levels across the interface line up. The potential variations away from the interface dipole layer introduced by the space charge layer are slow (on the order of magnitude of $\sim 0.5(V)$ within hundreds of nm or longer) due to the small percentage of dopant atoms.[27] This leads to the picture of band shift following electrostatic potential change since such potential variation occurs on a length scale much longer than the semiconductor unit cell size.

The band lineup at the planar metal-semiconductor interface is determined by the overall charge neutrality condition and the corresponding one-dimensional electrostatic considerations: $Q_m + Q_{is} + Q_{sc} = 0$, where Q_m, Q_{is} and Q_{sc} are the surface charge density within the metal (m) surface layer, semiconductor surface layer due to the interface states (is) and semiconductor space-charge (sc) layer respectively, which are obtained by averaging the three-dimensional charge density over the plane parallel to the interface. For n(p)-type semiconductor, the Schottky barrier height V_b for electron (hole) injection is determined by E_F and the conduction (valence) band edge. Since electrons can easily tunnel through the interface dipole layer, current tranport occurs by charge carriers injected into the bulk conduction/valence band states by tunneling through or thermionically emitted over the interface barrier. So the Schottky barrier height alone can be used for characterizing the transport characteristics.[27]

Two key concepts thus underlie the analysis of Schottky barrier formation at the planar metal-semiconductor interface: (1) The separation into the interface region (dipole layer) and the bulk semiconductor region (including the space-charge layer) with well-defined Fermi-level; (2) The rigid band shift following the local electrostatic potential change due to the planar interface structure. Both concepts are not valid in analyzing Schottky barrier formation at metal-SWNT interfaces.

B. Electrostatics of the metal-SWNT molecule interface

The calculated charge transfer and electrostatic potential change at the gold-SWNT-gold and titanium-SWNT-titanium junctions are shown in Figs. 6-8 for metal-SWNT distance of $\Delta L = 2.0, 2.5, 3.0(\mathring{A})$ respectively. The electrostatic potential change is obtained as the difference between electrostatic potentials within the metal-SWNT-metal junction and the bare SWNT molecule, which is calculated from the transferred charge throughout the SWNT using Eq. 6. Due to the molecular-scale dimension of both the SWNTs and the contact area, the transferred charge across the interface is confined in a finite region. Unlike the dipole *layer* at the bulk metal-semiconductor interface which induces a step-wise change in the electrostatic potential, the transferred charge across the metal-SWNT interface takes the form of molecular-size dipole, the electrostatic potential of which *decays to zero in regions far away from the interface*.[23,24] In addition, the SWNT molecule is undoped. The occupation of the electron states within the SWNT is determined by the Fermi-level of the electrodes, even for a long SWNT which has reached the bulk limit and a Fermi-level can be defined from the bulk band structure.

Note that despite the delocalized nature of SWNT electron states in the conduction/valence band, for a given metal-SWNT distance ΔL, both the magnitude and the range of the charge transfer at the metal-SWNT molecule interface are approximately independent of the SWNT length, reflecting the localized nature of interfacial charge transfer process[49,50] The charge transfer adjacent to the metal-SWNT interface shows Friedel-like oscillation.[78] Such Friedel-like oscillations of transferred charge have also been observed in planar metal-semiconductor interfaces,[80] finite atomic chains[81] and molecular tunnel junctions.[49,50] The oscillation of the interface-induced charge transfer dies out quickly inside the SWNTs as the length of the SWNT molecule increases. The oscillation in both the transferred charge and electrostatic potential change in the middle of the SWNT are due to the intrinsic two-sublattice structure of the zigzag tube, and persist in an infinitely long zigzag tube.[46,83]

As ΔL increases from $2.0\mathring{A}$ to $3.0\mathring{A}$, the magnitude of the charge transfer oscillation at the interface decreases with the decreasing interface coupling strength, but the magnitude of charge transfer inside the SWNT molecule is almost independent of the coupling strength across the interface. For the Au-SWNT-Au junction, there is a small positive charge transfer of 4.9×10^{-4} per atom in the middle of the 60-unitcell SWNT, while for the Ti-SWNT-Ti junction, there is instead a small negative charge tranfer of -6.5×10^{-5} per atom.[82]

Due to the long-range Coulomb interaction, the electrostatic potential change is determined by the transfered charge throughout the metal-SWNT-junction (Eq. 6). For a given metal-SWNT distance ΔL, its magnitude in the middle of the SWNT increases with the increasing SWNT size although the charge transfer is small except at the several layers immediately adjacent to the electrodes. The magnitude of the potential change in the interior of the SWNT saturates at the same length where the finite SWNT approaches the bulk limit, i.e., 50 unit cells corresponding to a length of $21.1(nm)$, for both Au-NT-Au and Ti-NT-Ti junctions. For a given metal-SWNT distance ΔL, the magnitude of the potential shift at the metal-SWNT interface is approximately constant for all the finite SWNTs studied.

The contact-induced charge transfer processes are often characterized as "charge-tranfer doping". If we follow the common practice in literature, the SWNT is "hole-doped" by contacting to gold (high work function) and "electron-doped" by contacting to titanium (low work function) electrode. Here it is important to recognize the difference in the physical processes governing the short-range and long-range electrostatics of the metal-SWNT interface. The charge transfer close to the metal-SWNT interface reflects the bonding configuration change upon contact to the metallic surfaces, which cannot contribute directly to transport since the corresponding charge distribution is localized[49,50]. Moving away from the interface, the effect due to the metal-SWNT coupling is reduced. For the longer SWNT molecule which has approached the bulk limit, the effect of the interface coupling on the electron states in the middle of the SWNT can be essentially neglected. However, since the electron occupation is determined by the Fermi-Dirac distribution of the metallic electrodes, the charging state in the interior of the SWNT which has approached the bulk limit is determined by the lineup of the SWNT bands relative to the metal Fermi-level, which in turn is determined by the self-consistent potential shift across the metal-SWNT-metal junction. Within the coherent transport regime, the transfered charge in the interior affects current indirectly by modulating the potential landscape acrosss the metal-SWNT-metal junction, which determines the electron transmission coefficient through Eq. 7.

A common feature of previous theoretical work on carbon nanotube devices is the use of the electrostatics of an ideal cylinder,[22,23,24,26,43] which neglects the electrostatic potential variation across the narrow region around the cylindrical surface where the π-electron density is non-negligible. However, the electrostatics of *any nanostructure is three-dimensional*. For the cylindrical SWNT, this means that the electrostatic potential across the SWNT junction varies both parallel and perpendicular to the NT axis and on the atomic-scale. This is clearly seen from the three-dimensional plot of the electrostatic potential change in Fig. 9. For the $(10, 0)$ SWNT with a diameter of $\approx 0.8(nm)$, the variation of the charge transfer-induced electrostatic potential change inside the SWNT cylinder is small, but decays to about 1/4 of its value at the cylindrical center $1(nm)$ away from the SWNT surface for both the Au-SWNT-Au and Ti-SWNT-Ti junctions.

The confined cylindrical geometry and three-dimensional electrostatics of the metal-SWNT interface lead to a

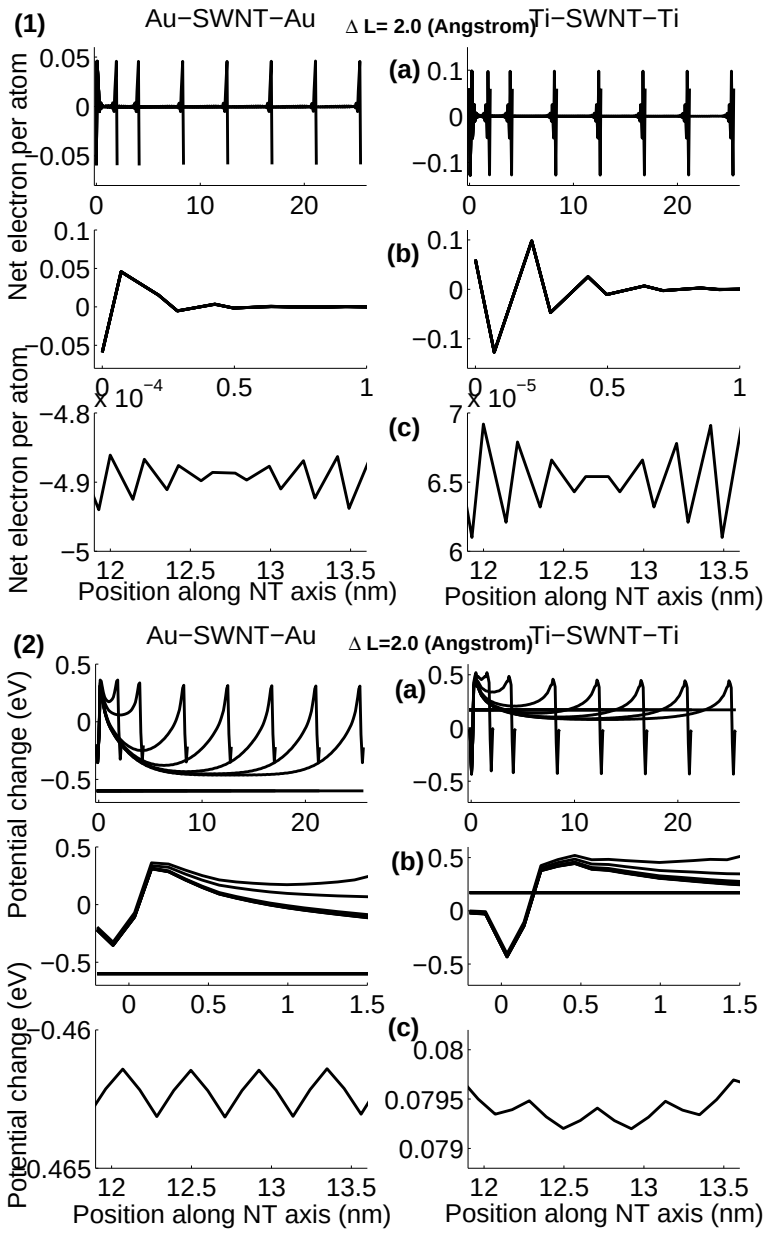

FIG. 6: Charge transfer (1) and electrostatic potential change (2) at the Au-finite SWNT-Au and Ti-finite SWNT-Ti junctions as a function of SWNT length for seven different lengths at SWNT-metal distance of $\Delta L = 2.0(\mathring{A})$. For each junction, we have also shown the magnified view both at the metal-SWNT interface (b) and in the middle of the longest (25.4 nm) SWNT molecule (c). The horizontal lines in the potential plot (2) denote the work function differences between the electrodes and the bulk SWNT.

profound change in the physical picture of the band shift, which applies to both finite SWNT molecules and long SWNT wires.[45,46] In particular, the shift of the local density of states along the nanotube axis *does not follow* the change in the electrostatic potential along the nanotube axis, although this is commonly assumed in the literature. This is illustrated in the three-dimensional plot of the LDOS as a function of position along NT axis in Fig. 10. Note that although the electrostatic potential varies by an amount $\geq 0.5(eV)$ going from the metal-SWNT interface to the middle of the 60-unit cell SWNT molecule for both junctions (Fig. 7), there is almost no shift of the conduction and valence band edge going from the interface to the middle of the SWNT molecule. This is in contrast with the planar metal-semiconductor interface, where the band shift away from the interface dipole layer follows the electrostatic potential change since it varies only in one direction *and* on a length scale large compared to the corresponding unit cell size.

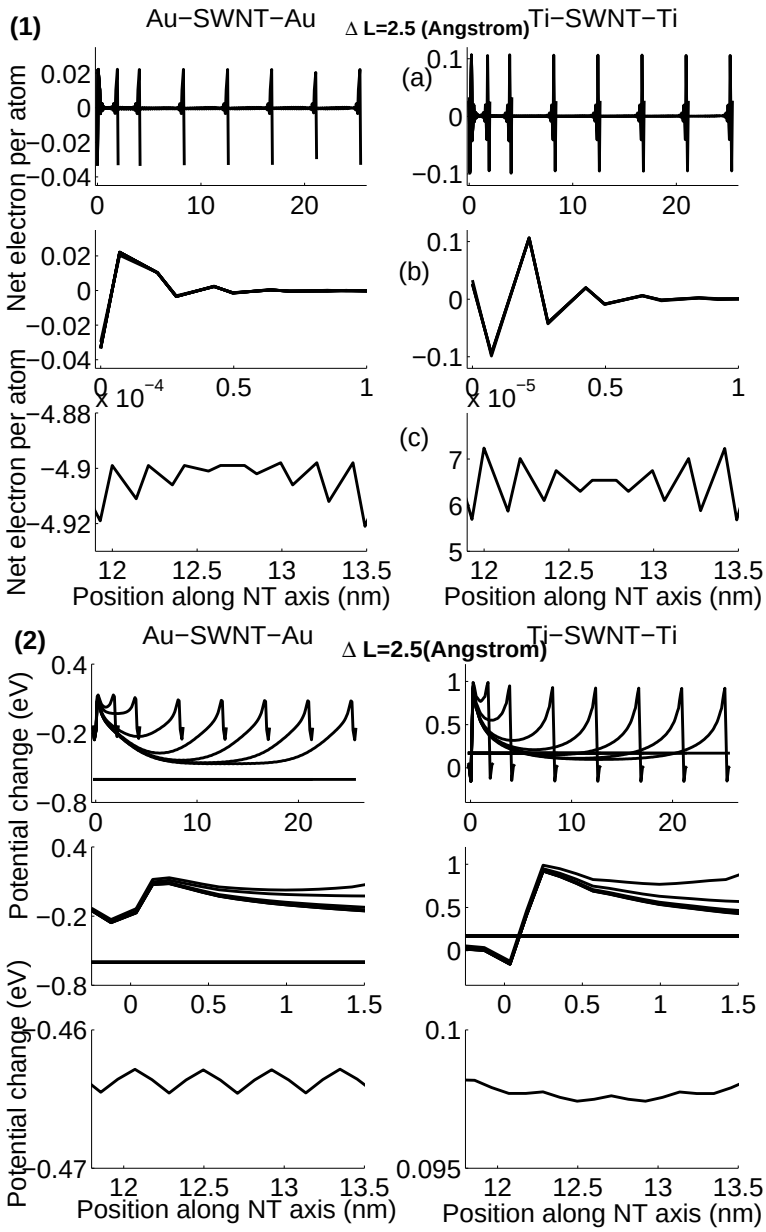

FIG. 7: Charge transfer (1) and electrostatic potential change (2) at the Au-finite SWNT-Au and Ti-finite SWNT-Ti junctions as a function of SWNT length for seven different lengths at SWNT-metal distance of $\Delta L = 2.5(\mathring{A})$. For each junction, we have also shown the magnified view both at the metal-SWNT interface (b) and in the middle of the longest (25.4 nm) SWNT molecule (c). The horizontal lines in the potential plot (2) denote the work function differences between the electrodes and the bulk SWNT.

The lack of connection between band shift and electrostatic potential change along the SWNT axis is obvious considering the 3-d nature of the electrostatics: Since the electrostatic potential change varies strongly in the direction perpendicular to the SWNT axis where the carbon pi-electron density is significant, there is no simple connection between the band shift and the electrostatic potential change at the cylindrical surface of the SWNT or at any other distance away from the SWNT axis. The relevant physics can be understood as follows: For the nanoscale SWNT considered here, the molecular-size interface dipole induces a long-range three-dimensional electrostatic potential change of $\sim 0.5(eV)$ within $\sim 5(nm)$ of the interface, which is much weaker than the atomic-scale electrostatic potential variation within the bare SWNT. Since the LDOS of the SWNT junction is obtained from the Hamiltion corrected by the charge transfer-induced electrostatic potential change, we can expect the effect on the spatial variation of the LDOS away from the interface due to such correction is small compared to the strong atomic-scale potential

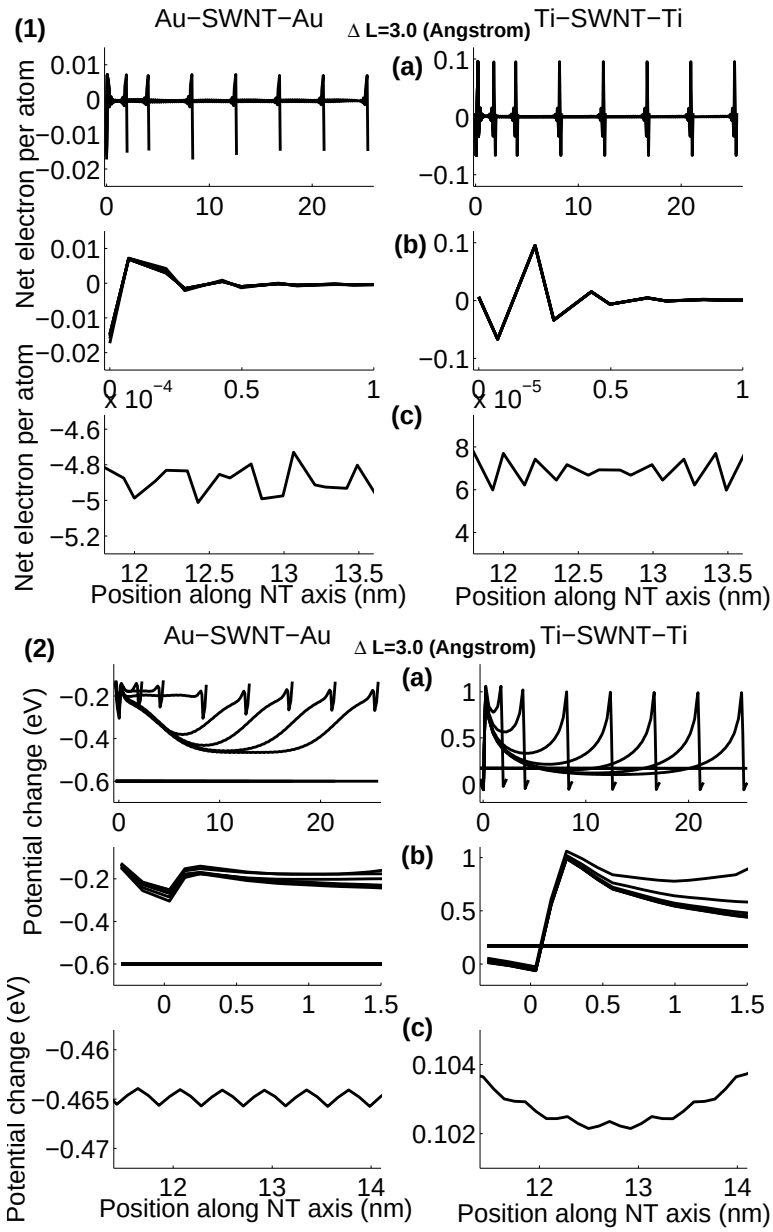

FIG. 8: Charge transfer (1) and electrostatic potential change (2) at the Au-finite SWNT-Au and Ti-finite SWNT-Ti junctions as a function of SWNT length for seven different lengths at SWNT-metal distance of $\Delta L = 3.0(\mathring{A})$. For each junction, we have also shown the magnified view both at the metal-SWNT interface (b) and in the middle of the longest (25.4 nm) SWNT molecule (c). The horizontal lines in the potential plot (2) denote the work function differences between the electrodes and the bulk SWNT.

variations included implicitly in the initial Hamiltonian H_0. The effect of the electrostatic potential change on the LDOS in regions within $\sim 5(nm)$ of the metal-SWNT interface is thus similar to that of small molecules in molecular tunnel junctions, where detailed studies in Ref. 50 have shown that the charge transfer-induced electrostatic potential change in the molecular junction doesn't lead to a rigid shift of the molecular energy levels (or band edges), but can have different effects on different molecular states (or band structure modification) depending on their charge distributions.

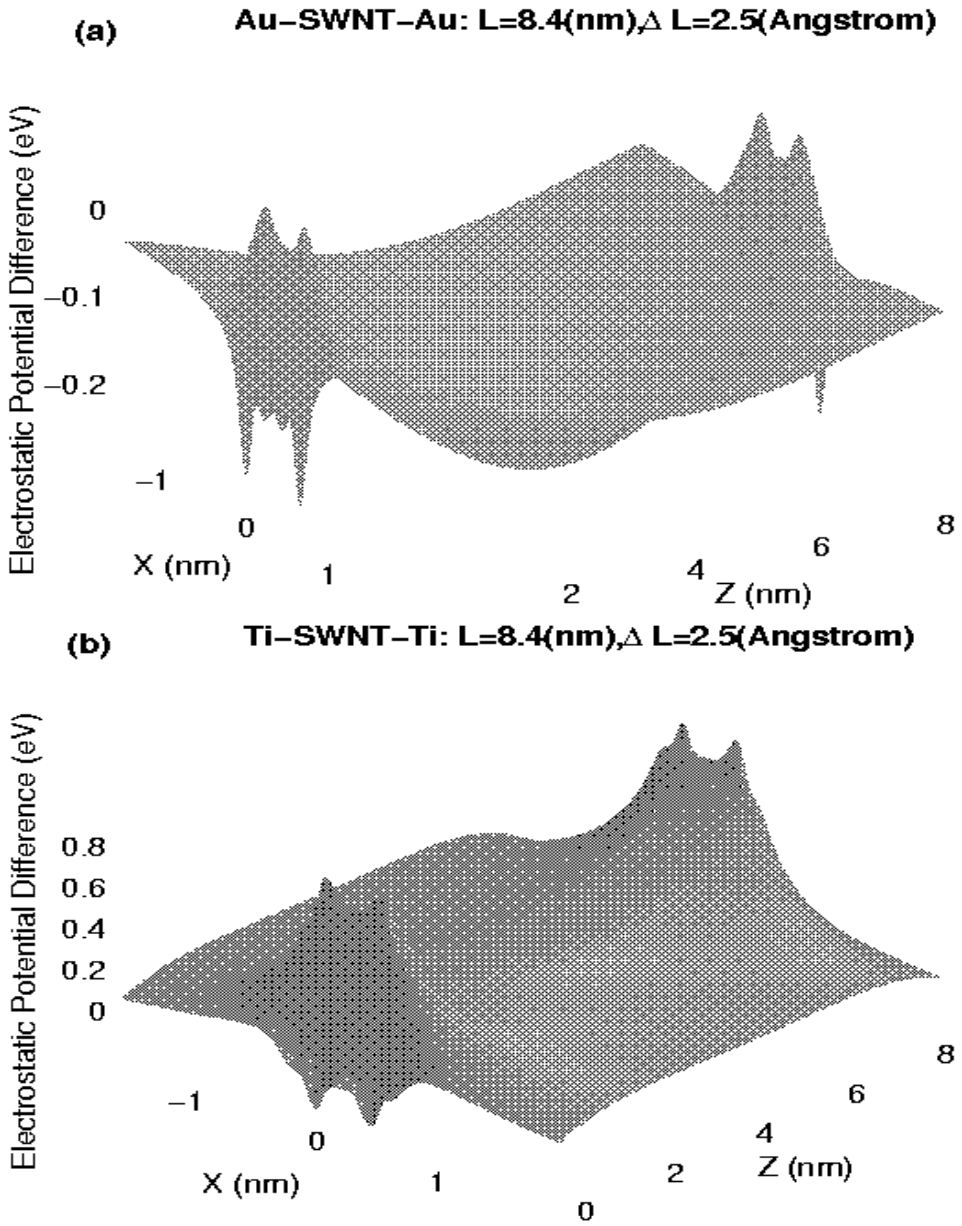

FIG. 9: (Color online) Cross sectional view of electrostatic potential change at the Au-SWNT-Au (upper figure) and Ti-SWNT-Ti junction (lower figure) for SWNT molecule length of $8.4(nm)$ and metal-SWNT distance of $\Delta L = 2.5(\AA)$. The SWNT diameter is $0.78(nm)$. The electrostatic potential change shown here is induced by the charge transfer across the interface and calculated using Eq. 6.

C. "Band" lineup and electron transmission across the metal-finite SWNT molecule interface

For a planar metal-semiconductor interface, the band lineup is determined once the electrostatic potential drop across the interface is known. The horizontal lines in the potential plots of Figs. 6-8(b) denote the work function differences between the electrodes and the bulk SWNT. For a bulk metal-semiconductor interface, this would have given the magnitude of the potential shift which aligns the Fermi-level across the interface. But for the metal-finite SWNT interface considered here, the band lineup should be determined from the local density of states (LDOS) in the middle of the SWNT. This is shown in Fig. 11 for both Au-SWNT-Au and Ti-SWNT-Ti junctions.

The "band" lineup relevant to the transport characteristics can also be determined equivalently from the electron transmission characteristics of the equilibrium metal-SWNT-metal junction, which is calculated using Eq. 7 and depends on the surface electronic structure, the coupling across the interface and the electronic structure of the

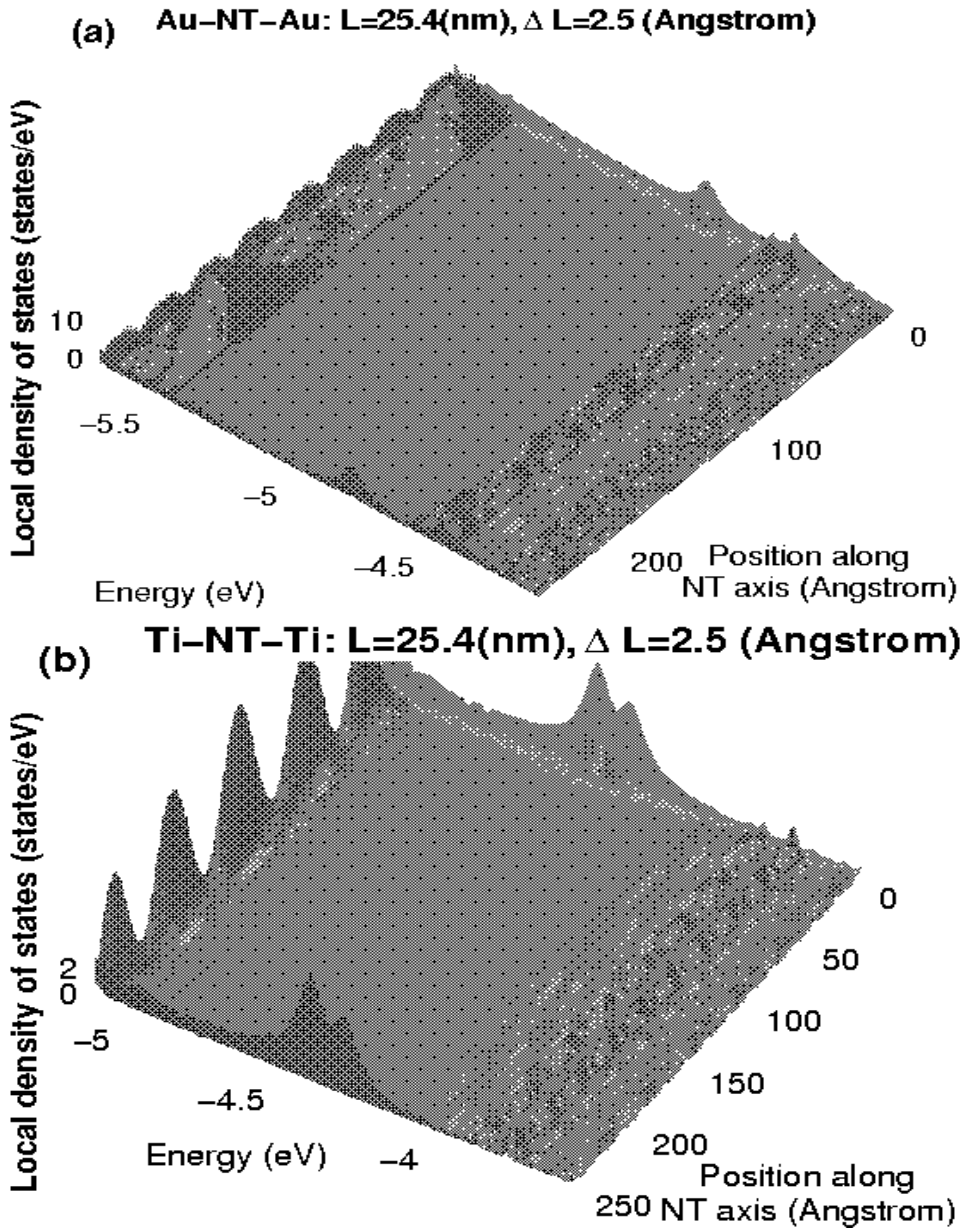

FIG. 10: (Color online) Three-dimensional plot of the local density of states at the Au-SWNT-Au (a) and Ti-SWNT-Ti (b) junctions as a function of position along the NT axis for SWNT length of $25.4(nm)$ and metal-SWNT distance of $\Delta L = 2.5(\mathring{A})$. Note that the sharp peaks around $-4.5(eV)$ due to the dangling bond state at the ends of the isolated SWNT (Fig. 4(b)) have been replaced by broadened peaks within the band gap due to the MIGS at the metal-SWNT molecule interface.

SWNT molecule. The surface density of states of the bare gold and titanium electrodes calculated using tight-binding parameters[74] are shown in Fig. 12, while the transmission characteristics of the metal-SWNT-metal junctions are shown in Fig. 13. For the shortest SWNT in the molecular limit ($2.0nm$), there is significant transmission around the metal Fermi-level E_f which is suppressed rapidly with increasing SWNT length. The difference in the electron transmission through the SWNT conduction band region in the Au-SWNT-Au and Ti-SWNT-Ti junctions is mostly due to the difference in the electrode band structures above E_f (sp-band for Au and d-band for Ti).

From both the LDOS and transmission characteristics of the 60-unit cell SWNT, we can determine that for the Au-SWNT-Au junction the Fermi-level location goes from slightly below (by ~ 0.1 eV) the mid-gap of the 60 unitcell SWNT to the mid-gap as the gold-SWNT distance increases from $2.0(\mathring{A})$ to $3.0(\mathring{A})$. For the Ti-SWNT-Ti junction, the Fermi-level location goes from above (by ~ 0.25 eV) the mid-gap of the 60-unit cell SWNT molecule to the midgap as the titanium-SWNT distance increases from $2.0(\mathring{A})$ to $3.0(\mathring{A})$. Note that this value is approximately the same for

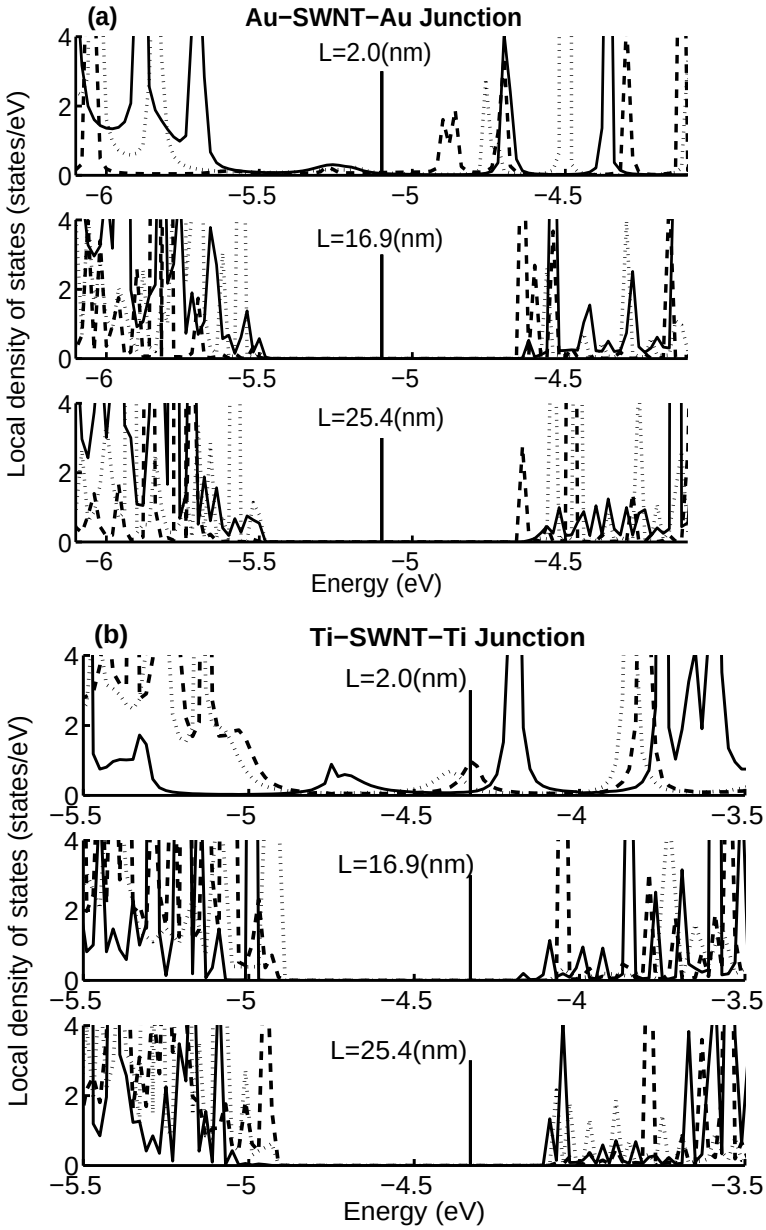

FIG. 11: Local density of states at the middle of the Au-SWNT-Au junction (a) and Ti-SWNT-Ti junction (b) for SWNT length of $2.0, 16.9$ and $25.4(nm)$ respectively. Solid line: $\Delta L = 2.0(\AA)$. Dotted line: $\Delta L = 2.5(\AA)$. Dashed line: $\Delta L = 3.0(\AA)$. The vertical lines show the position of the metal Fermi-level.

SWNTs longer than 40-unit cell (16.9 nm), i.e., the same length where the magnitude of the electrostatic potential change in the middle of the SWNT begins to saturate (Figs. 6-8(b)).

The physical principles of Schottky barrier formation at the metal-SWNT molecule interface can thus be summarized as follows: Since the effect of the interface perturbation on the electron states inside the SWNT molecule is small, for the SWNTs that are long enough to approach the bulk limit, the metal Fermi-level position should be close to the middle of the gap since otherwise extensive charge transfer will occur inside the SWNT junction. Since the screening of the work function difference inside the SWNT junction is weak, the metal Fermi-level should be below (above) the middle of the gap for a high (low) workfunction metal so that the net decrease (increase) of electrons inside the SWNT molecule shifts the SWNT band edge down (up) relative to the metal Fermi-level. Exactly how this is achieved from the interface to the middle of the channel will depend on the details of the contact (types of metal and strength of interface coupling). At the weak coupling limit, the lineup of the Fermi-level for the SWNT molecules which have reached the bulk limit is such that the perturbation of the electron states inside the SWNT molecule is minimal,

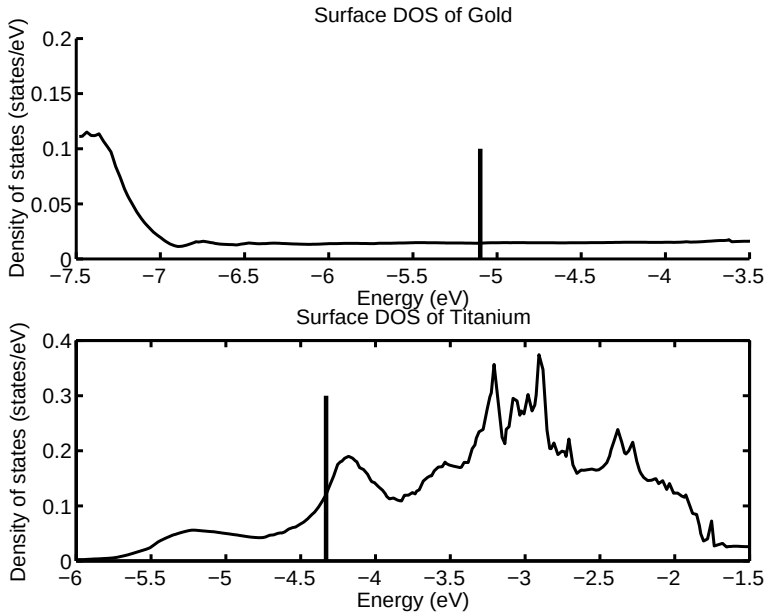

FIG. 12: Surface density of states of the gold and titanium electrodes. The vertical lines show the position of metal Fermi-level.

i.e., at mid-gap. Note that since the LDOS around the midgap is negligible inside the SWNT, the magnitude of the transfered charge in the middle of the SWNT molecule is approximately independent of the interface coupling strength despite the different band lineup scheme at three different metal-SWNT distances (Figs. 6-8(a)).

V. LENGTH AND TEMPERATURE DEPENDENCE OF THE CONDUCTANCE OF THE METAL-SWNT MOLECULE INTERFACE

Given the electrostatic potential change ΔV across the metal-SWNT interface, we can caculate the length and temperature dependence of the metal-SWNT-metal junction conductance using Eq. 12. The length dependence of the junction conductance at room temperature is shown in Fig. 14 for both Au-SWNT-Au and Ti-SWNT-Ti junctions at the three metal-SWNT distances. We have separated the junction conductance into the tunneling and thermal-activation contributions as discussed in sec. II A.

The tunneling conductance (also the zero-temperature conductance) for both junctions decreases exponentially with the SWNT length for SWNT longer than $4.1(nm)$ (Fig. 14), where the perturbation of the electron states inside the SWNT due to the interface coupling can be neglected. The exponential decay with length for tunneling across a finite molecular wire in contact with two metal electrodes has been analyzed in detail in recent literature using either simple tight-binding theory[84] or complex band structures calculated from first-principles theory.[85] But the essential physics can be captured from the simple WKB picture of tunneling through potential barriers with constant barrier height. A separation of the contact and molecule core effect on the tunneling resistance can thus be achieved using the functional relation $R = R_0 e^{dL}$, where R_0 is the contact resistance and d is the inverse decay length for tunneling across the SWNT molecule. We find that the Au-SWNT-Au junction has the contact resistance $R_0 = 0.115, 1.88, 2.59(M\Omega)$ and inverse decay length of $d = 1.68, 1.68, 1.68(1/nm)$ for the Au-SWNT distance of $\Delta L = 2.0, 2.5, 3.0(\AA)$ respectively. The Ti-SWNT-Ti junction has the contact resistance $R_0 = 0.023, 3.14, 4.95(M\Omega)$ and inverse decay length of $d = 1.51, 1.52, 1.53(1/nm)$ for the Ti-SWNT distance of $\Delta L = 2.0, 2.5, 3.0(\AA)$ respectively. Note that the contact resistance increases rapidly with the increasing metal-SWNT distance due to the reduced interface coupling, but the inverse decay length (which is a bulk-related parameter) remains approximately constant.[85] The total conductance of the metal-SWNT-metal junction at room temperature saturates with increasing SWNT length. This is due to the fact that the potential shift extends over a range comparable to the half of the SWNT length until the SWNT reaches the bulk limit. For longer SWNT, the tunneling is exponentially suppressed while the transport becomes dominated by thermal activation over the potential barrier whose height is approximately constant for all the SWNTs investigated.

The length and temperature dependence of the metal-finite SWNT-metal junction can also be seen more clearly from Fig. 15, where we show the conductance of the SWNT junction as a function of temperature for lengths of 2.0,

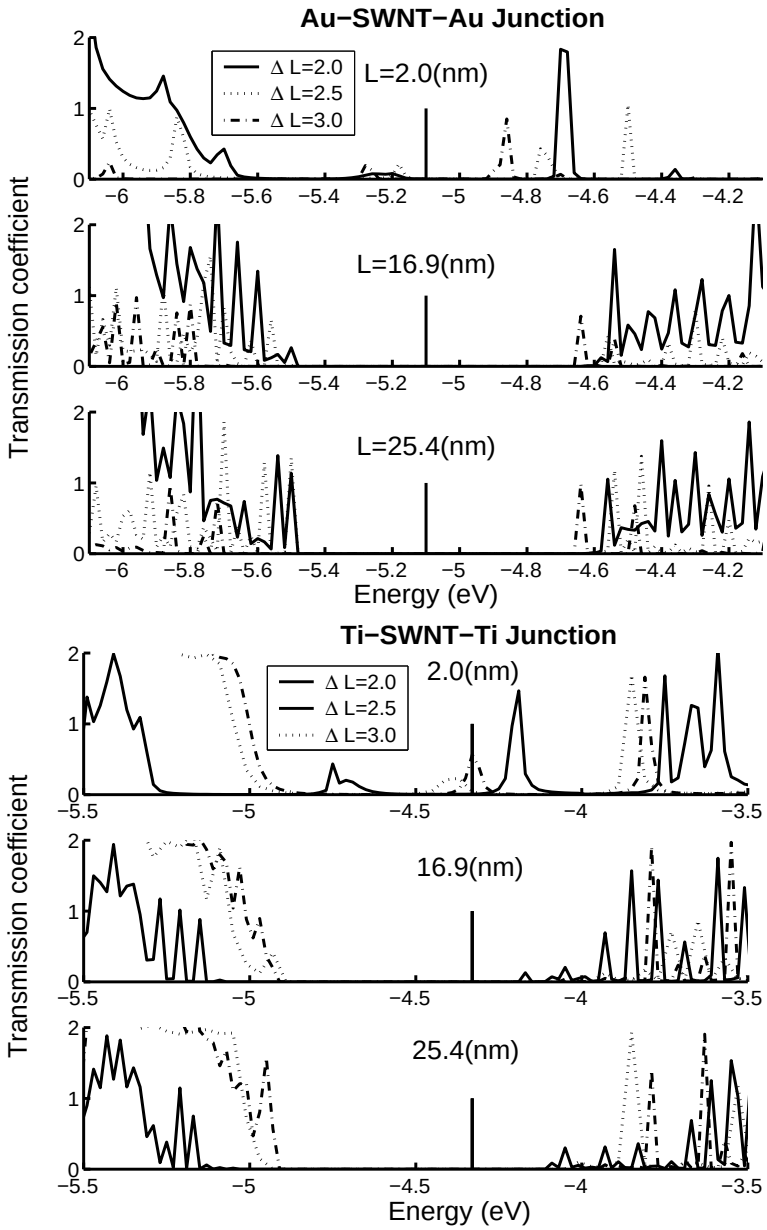

FIG. 13: Electron transmission characteristics of the Au-SWNT-Au (upper figure) junction and Ti-SWNT-Ti (lower figure) junction for SWNT length of $2.0, 16.9$ and $25.4(nm)$ and metal-SWNT distance of $2.0, 2.5$ and $3.0(\mathring{A})$ respectively. The vertical lines show the position of the metal Fermi-level at each junction.

8.4 and 16.9 (nm) in both Au-SWNT-Au and Ti-SWNT-Ti junctions and in the strong coupling limit ($\Delta L = 2.0\mathring{A}$). For the shortest SWNT molecule (2.0 nm) studied, both tunneling and thermal contributions to the conductance at room-temperature are significant. So the condutance increases only by a factor of 2 going from $100(K)$ to $250(K)$ for the Ti-SWNT-Ti junction and is almost temperature independent for the Au-SWNT-Au junction. The thermionic-emission contribution begins to dominate over the tunneling contribution at SWNT length of 8.4 (nm) and longer, correspondingly the increase of conductance with temperature is faster. But overall the temperature dependence is much weaker than the exponential dependence in, e.g., electron transport through the planar metal-semiconductor interfaces.[86]

The length and temperature dependence of the SWNT molecule junction can be understood rather straightforwardly using the Breit-Wigner formula,[87] first introduced by Buttiker[88] for electron transmission through double-barrier tunneling structures. For electron transmission within the energy gap between the highest-occupied-molecular-orbital (HOMO) and lowest-unoccupied-molecular-orbital (LUMO) of the SWNT molecule, we can approximate the energy

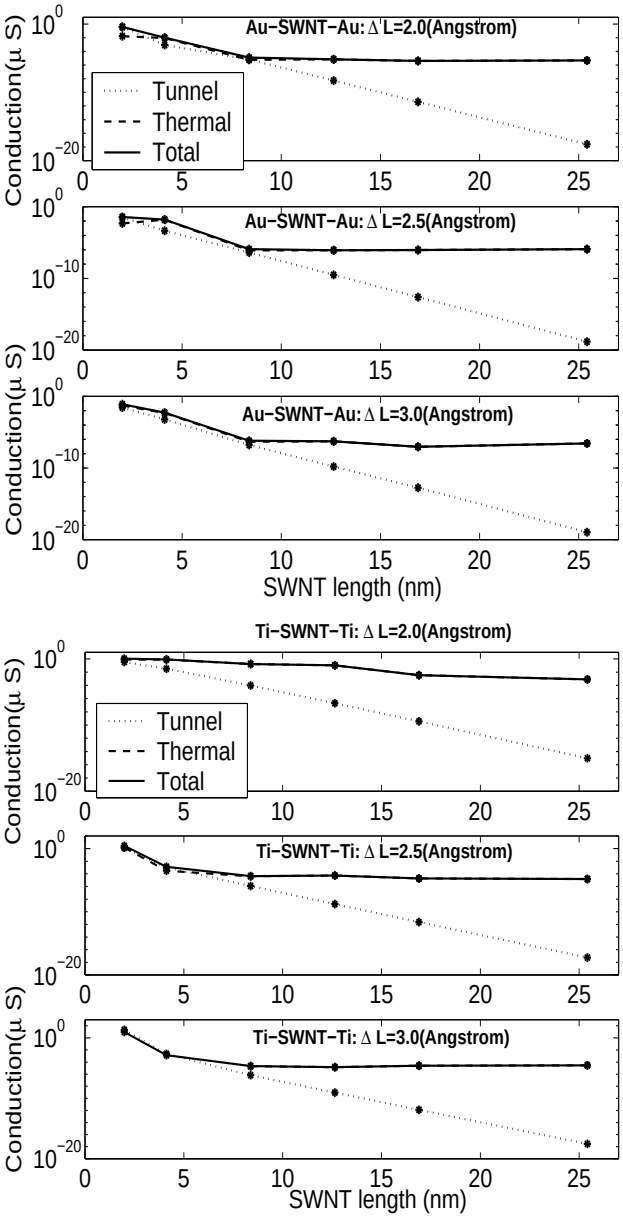

FIG. 14: Room temperature conductance of the Au-SWNT-Au (upper figure) junction and Ti-SWNT-Ti (lower figure) junction as a function of the SWNT length at three different metal-SWNT distances.

dependence of the transmission coefficient as

$$T(E) \approx \sum_{i=HOMO,LUMO} \frac{\Gamma_{i;L}\Gamma_{i;R}}{(E-E_i)^2 + 1/4(\Gamma_{i;L}+\Gamma_{i;R})^2} \tag{13}$$

where $\Gamma_{i;L(R)}$ (i=HOMO,LUMO) is the partial width of resonant transmission through the HOMO (LUMO) level due to elastic tunneling into the left (right) electrode respectively. Note that as the SWNT molecule reaches the bulk limit, the HOMO and LUMO levels give the valence band and conduction band edge respectively. For given SWNT molecule and metallic electrodes, $\Gamma_{HOMO(LUMO);L(R)}$ is constant. The increase of transmission coefficient with energy from the Fermi-level E_f towards the relevant band edge is thus of Lorentzian form, which is also generally true for nanostructures with only a finite number of conduction channels. From Eq. 12, the temperature dependence of the conductance is thus determined by the tail of the Lorentzian around E_f averaged over a range $\sim kT$ due to the thermal broading with the corresponding weight $\frac{df}{dE}(E-E_f) = exp((E-E_f)/kT)/(kT(exp((E-E_f)/kT)+1)^2)$.

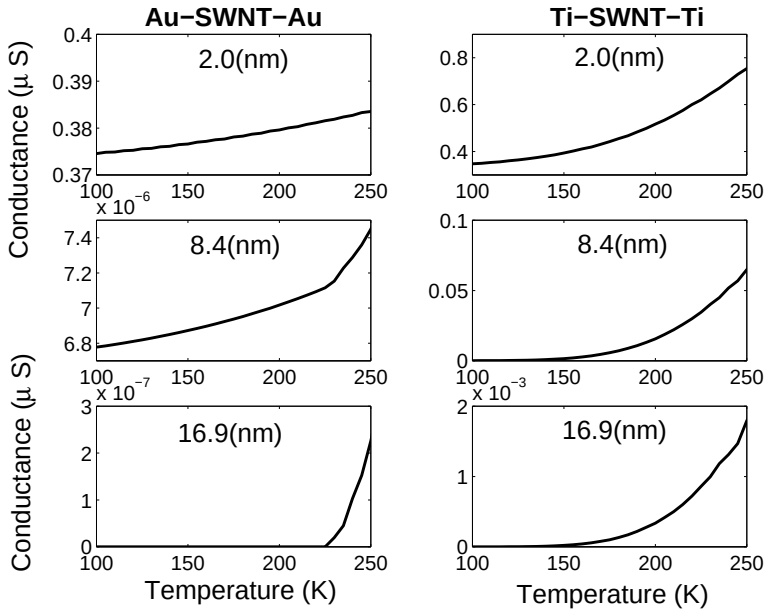

FIG. 15: Temperature dependence of the conductance of the Au-SWNT-Au (left figure) junction and Ti-SWNT-Ti (right figure) junction as a function of the SWNT length at metal-SWNT distance of $\Delta L = 2.0(\mathring{A})$.

This leads to much weaker-than-exponential dependence on temperature of the junction conductance, as compared to the metal-semiconductor interface, where the exponential dependence of conductance on temperature is due to the exponential decrease of carrier densities with energy large enough to overcome the interface barrier.[27] As the length of the SWNT molecule increases, the partial width $\Gamma_{HOMO(LUMO);L(R)}$ due to tunneling into the electrodes decreases exponentially (from the WKB approximation,[88]) leading to the exponential dependence on junction length of the tunneling conductance.

VI. CURRENT-VOLTAGE CHARACTERISTICS OF THE METAL-FINITE SWNT INTERFACE

In principle, to calculate the current-voltage characteristics of the metal-SWNT-metal junction, a self-consistent calculation of the charge and potential response will be needed at each bias voltage to take into account the screening of the applied electric field within the junctions.[50,89] This is computationally demanding even for the self-consistent tight-binding method due to the large size of the SWNT molecule. Therefore, in this section we calculate the current-voltage characteristics using three different models of the electrostatic potential profiles in the metal-finite SWNT-metal junction in order to illustrate qualitatively the importance of the proper modeling of the self-consistent screening of the applied source/drain bias voltage.[50,61,63,64] The fully self-consistent current transport is under investigation and will be reported in future publications.

The three potential response models we choose are: (1) We assume all the voltage drop occurs at the metal-SWNT interface with the two interface contributing equally (Model 1); (2) We assume the voltage drop across the metal-SWNT-metal junction is piece-wise linear (Model 2); (3) We assume the voltage drops linearly across the entire metal-SWNT-metal junction (Model 3). The three potential models chosen here represent the source/drain field configuration at three different limits: In the absence of the SWNT molecule, we are left with the bare (planar) source/drain tunnel junction. For ideal infinitely conducting electrodes, the voltage drop will be linear with constant electric field across the source/drain junction. In general, sandwiching the SWNT molecule between the two electrodes leads to screening effect. If we neglect entirely the screening of the applied source/drain field by the SWNT molecule, we arrive at potential model 3. If the nanotube is infinitely conducting, we arrive at potential model 1. In practice, both the electrodes and the SWNT are not infinitely conducting, and the voltage drop can occur both across the metal-SWNT interface and inside the SWNT. Since the potential variation will be the largest close to the interface for the homogeneous SWNT assumed here, for model 2 we assume the potential profile is such that the magnitude of the field across the first unitcell of the SWNT at the two ends is 10 times of that in the interior of the SWNT molecule. Note that we have neglected the electrostatic potential variation in the direction perpendicular to the source/drain field. For SWNTs with cylindrical structure, this can be important in a fully self-consistent analysis of the nonlinear

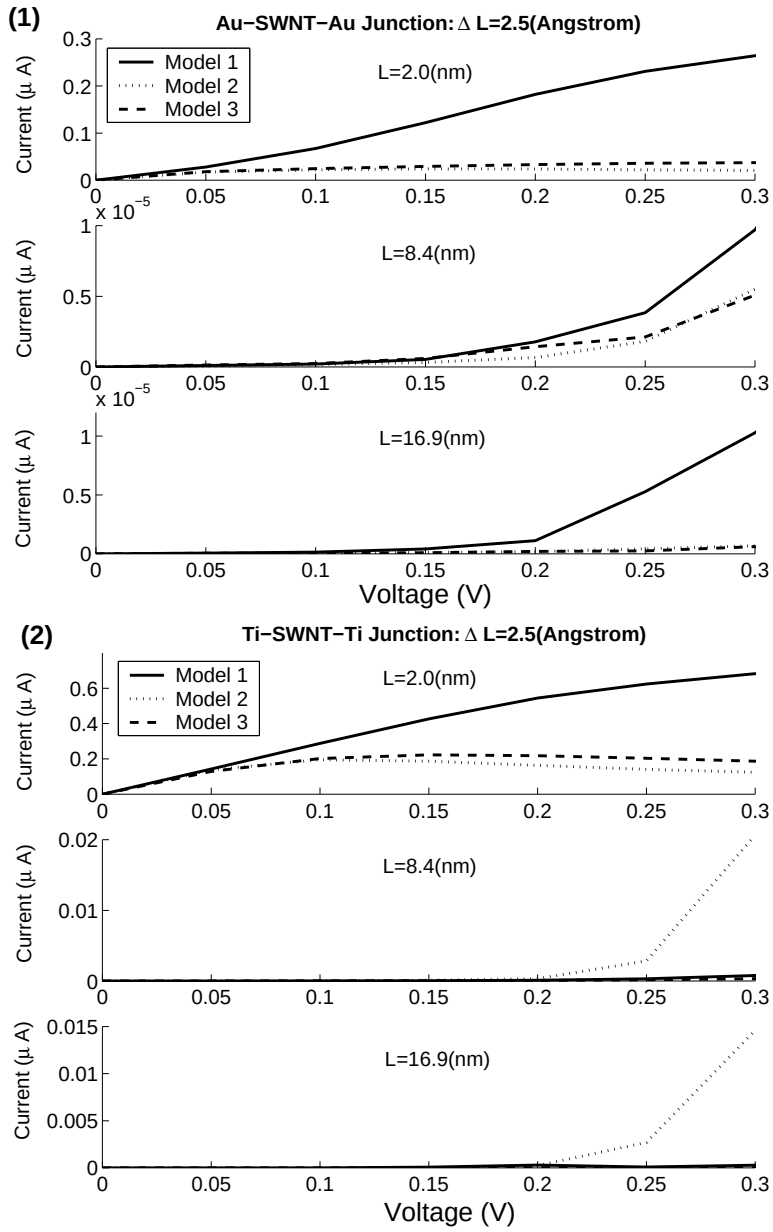

FIG. 16: Current-voltage characteristics of the Au-SWNT-Au (1) and the Ti-SWNT-Ti (2) junction for SWNT lengths of $2.0, 8.4, 16.9(nm)$ and metal-SWNT distance of $2.5(\mathring{A})$. We consider three different models of electrostatic potential profile within the SWNT junction.

current-voltage characteristics as we have seen in the previous sections. The three potential models chosen here are merely used to demonstrate the importance of the fully self-consistent study.

The calculated current-voltage (I-V) characteristics of the metal-SWNT-metal junctions for SWNT lengths of $2.1, 8.4, 16.9(nm)$ and metal-SWNT distance of $2.5(\mathring{A})$ are plotted in Fig. 16 for both junctions. For electrostatic potential models 2 and 3, the I-V characteristics are obtained by superposing the assumed electrostatic potential profile onto the Hamiltonian of the equilibrium junction and evaluating its matrix element by direct numerical integration. We find that as the length of SWNT increases, the three different models of electrostatic potential response lead to qualitatively different current-voltage characteristics in both the magnitude of the current and its voltage dependence. This is because current transport is dominated by thermal-activation contribution for all the SWNT molecules investigated except the shortest ones. For the Au-SWNT-Au junction, we find that potential models 2 and 3 give qualitatively similar I-V characteristics, indicating that potential drop within the SWNT bulk is important. But for the Ti-SWNT-Ti junction, we find that potential models 1 and 3 give qualitatively similar I-V characteristics for

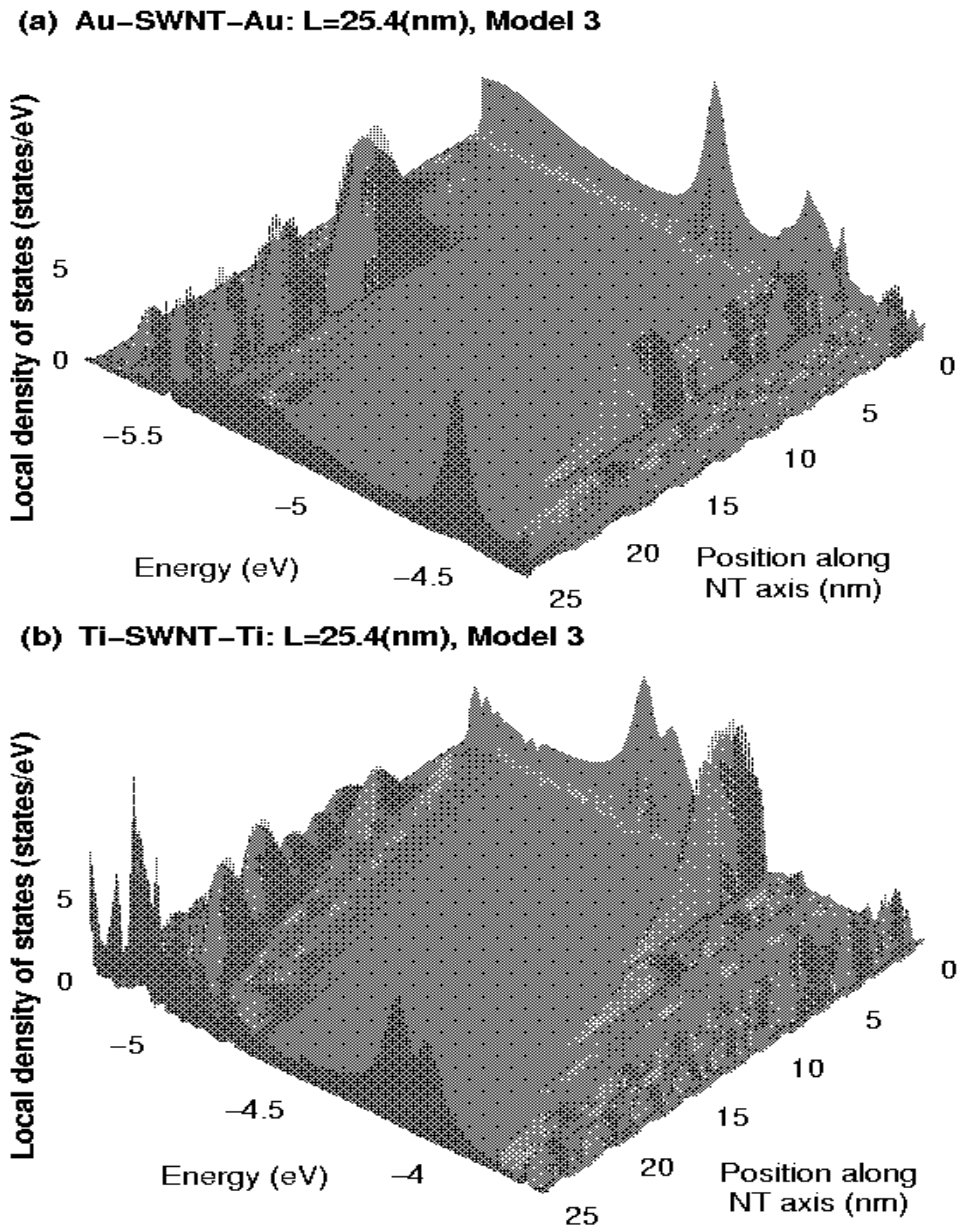

FIG. 17: (Color online) Three-dimensional plot of the local density of states at the Au-SWNT-Au (a) and Ti-SWNT-Ti (b) junctions as a function of position along the NT axis for SWNT length of $25.4(nm)$ and metal-SWNT distance of $\Delta L = 2.5(\mathring{A})$ at source/drain bias voltage of $0.5(V)$. We assume the voltage drops linearly across the SWNT junction (potential model 3).

SWNTs longer than $2.0(nm)$, indicating instead that potential drop across the metal-SWNT interface is important.

The contact dependence of the source/drain field effect can also be seen more clearly by analyzing its effect on the SWNT electronic structure from Fig. 17, where we show the three-dimensional plot of the LDOS of the SWNT within the Au-SWNT-Au and Ti-SWNT-Ti junctions at applied bias voltage of $0.5(V)$ and assuming potential model 3. Since for the equilibrium SWNT junction, the potential variation is appreciable over a length scale comparable to half of the SWNT length and up to $\sim 10(nm)$, both the magnitude and the voltage-dependence of the current will be sensitive to the spatial variation of the potential response to the applied voltage over the same length scale, which may have different effects on the SWNT band structure depending on the metallic electrodes used (Fig. 17). Therefore accurate modeling of this long-range potential variation at the metal-SWNT interface will be critical for evaluating the current-transport mechanism of the nanoscale SWNT devices.

VII. CONCLUSION

The rapid development of single-wall carbon nanotube-based device technology presents opportunities both for exploring novel device concepts based on atomic-scale nanoengineering techniques and for examining the physical principles of nanoelectronics from the bottom-up atomistic approach. As the first example of the device physics problems raised in this context, we examine electron transport through metal-SWNT interface when the finite SWNT is contacted to the metal surfaces through the dangling bonds at the end, which presents an atomic-scale analogue to the planar metal-semiconductor interface. Due to the quasi-one-dimensional geometry of the SWNTs, a correct understanding of the physical mechanisms involved requires an atomistic analysis of the electronic processes in the configuration of the metal-SWNT-metal junctions.

We have presented in this paper such a microscopic study of electronic and transport properties of metal-SWNT interfaces, as the length of the finite SWNT varies from the molecular limit to the bulk limit and the strength of the interface coupling varies from the strong coupling to the weak coupling limit. Our models are based on a self-consistent tight-binding implementation of the recently developed self-consistent matrix Green's function (SCMGF) approach for modeling molecular electronic devices, which includes atomistic description of the SWNT electronic structure, the three-dimensional electrostatics of the metal-SWNT interface and is applicable to arbitrary nanostructured devices within the coherent transport regime. We present a bottom-up analysis of the nature of the Schottky barrier formation, the length and temperature dependence of electron transport through the metal-SWNT interfaces, which show quite different behavior compared to the planar metal-semiconductor interfaces, due to the confined cylindrical geometry and the finite number of conduction channels within the SWNT junctions. We find that the current-voltage characteristics of the metal-SWNT-metal junctions depend sensitively on the electrostatic potential profiles across the SWNT junction, which indicates the importance of the self-consistent modeling of the long-range potential variation at the metal-SWNT interface for quantitative evaluation of device characteristics.

Much of current interests on the Schottky barrier effect at metal-SWNT interface are stimulated by the controversial role it plays in the operation of carbon nanotube field-effect transistors (CNTFET),[30,31,32] where different contact schemes and metallic electrodes have been used. In general, the operation of CNTFET will be determined by the combined gate and source/drain voltage effect on the Schottky barrier shape at the metal-SWNT interface, which may depend on the details of the metal-SWNT contact geometry, nanotube diameter/chirality and temperature/voltage range. Correspondingly, an atomic-scale understanding of the gate modulation effect within the metal-insulator-SWNT capacitor configuration will also be needed, similar to the planar metal-oxide-semiconductor structure.[90] We believe that detailed knowledges of the electronic processes within both the metal-SWNT-metal junction and the metal-insulator-SWNT capacitor are needed before a clear and unambiguous picture on the physical principles governing the operation of CNTFET can emerge. In particular, preliminary theoretical results on the carbon-nanotube field-effect transistors show that for SWNT molecule end-contacted to the electrodes, the nanotube transistor functions through the gate modulation of the Schottky barrier at the metal-SWNT interface (in agreement with recent experiments,[30]) which becomes more effective as the length of the SWNT molecule increases. Further analysis is thus needed that treat both the gate and source/drain field self-consistently within the SWNT junctions, to achieve a thorough understanding of SWNT-based nanoelectronic devices.

Acknowledgments

This work was supported by the DARPA Moletronics program, the NASA URETI program, and the NSF Nanotechnology Initiative.

---

* Electronic address: yxue@uamail.albany.edu; URL: `http://www.albany.edu/~yx152122`
* Author to whom correspondence should be addressed.

[1] S.M. Sze, *Semiconductor Devices: Physics and Technology*, 2nd edition (Wiley, New York, 2002).
[2] L.L. Chang, L. Esaki and R. Tsu, Appl. Phys. Lett. **24**, 593 (1974).
[3] W. Shockley, Proc. IRE **40**, 1289 (1952).
[4] W. Shockley, *Electrons and Holes in Semiconductors* (Van Nostrand, New York, 1950); J.M. Luttinger and W. Kohn, Phys. Rev. **97**, 869 (1955).
[5] S.M. Sze, *Physics of Semiconductor Devices*, 2nd edition (Wiley, New York, 1981).
[6] *Hot Carrier in Semiconductor Nanostructures: Physics and Applications*, edited by J. Shah (Academic Press, San Diego, 1992); *Quantum Transport in Semiconductors*, edited by D.K. Ferry and C. Jacoboni (Plenum, New York, 1992).

[7] R.H. Dennard, F.H. Gaensslen, H.-N. Yu, V.L. Rideout, E. Bassous, and A.R. Leblanc, IEEE J. Solid-State Circuits **SC-9**, 256 (1974); D.J. Frank, R.H. Dennard, E. Nowalk, P.M. Solomon, Y. Taur, and H.-S.P. Wong, Proc. IEEE **89**, 259 (2001).

[8] W. Kohn and J.M. Luttinger, Phys. Rev. **108**, 590 (1957); W. Shockley, Bell Syst. Tech. J. **28**, 435 (1949); W. van Roosbroeck, *ibid.* **29**, 560 (1950); R. Stratton, Phys. Rev. **126**, 2002 (1962).

[9] W. Hänsch, *The Drift Diffusion Equation and Its Applications in MOSFET Modeling* (Springer, Wien, 1991); M. Lundstrom, *Fundamentals of Carrier Transport*, 2nd edition (Cambridge University Press, Cambridge, 2000).

[10] F.S. Khan, J.H. Davies, and J.W. Wilkins, Phys. Rev. B **36**, 2578 (1987); L. Reggiani, P. Lugli, and A.P. Jauho, *ibid.* **36**, 6602 (1987); P. Lipavský, F.S. Khan, F. Abdolsalami, J.W. Wilkins, *ibid.* **43**, 4885 (1991).

[11] M. Lundstrom, IEEE Electron Device Lett. **18**, 361 (1997); S. Datta, F. Assad, and M.S. Lundstrom, Superlatt. Microsctruc. **23**, 771 (1997).

[12] S. Iijima and T. Ichihashi, Nature **363**, 603 (1993).

[13] C. Dekker, Phys. Today **52**(5), 22 (1999).

[14] R. Saito, G. Dresselhaus and M.S. Dresselhaus, *Physical Properties of Carbon Nanotubes* (Imperial College Press, London, 1998); C.T. White and J.W. Mintmire, Nature **394**, 29 (1998).

[15] P.L. McEuen, M.S. Fuhrer, and H. Park, IEEE Trans. Nanotech. **1**, 78 (2002); Ph. Avouris, J. Appenzeller, R. Martel, and S.J. Wind, Proc. IEEE **91**, 1772 (2003).

[16] S.J. Tans, A.R.M. Verschuen and C. Dekker, Nature **393**, 49 (1998); A. Bachtold, P. Hadley, T. Nakanishi and C. Dekker, Science **294**, 1317 (2001); S.G. Lemay, J.W. Janssen, M. van den Hout, M. Mooij, M.J. Broikowski, P.A. Willis, R.E. Smalley, L.P. Kouwenhoven and C. Dekker, Nature **412**, 617 (2001).

[17] R. Martel, T. Schmidt, H.R. Shea, T. Hertel and Ph. Avouris, Appl. Phys. Lett. **73**, 2447 (1998); R. Martel, V. Derycke, C. Lavoie, J. Appenzeller, K.K. Chan, J. Tersoff and Ph. Avouris, Phys. Rev. Lett. **87**, 256805 (2001).

[18] M. Bockrath, D.H. Cobden, J. Lu, A.G. Rinzler, R.E. Smalley, L. Balents and P.L. McEuen, Nature **397**, 598 (1999); J. Park and P. McEuen, Appl. Phys. Lett. **79**, 1363 (2001).

[19] J. Kong, H.T. Soh, A. Cassell, C.F. Quate, and H. Dai, Nature **395**, 878 (1998); C. Zhou, J. Kong, and H. Dai, Appl. Phys. Lett. **76**, 1597 (2000); C. Zhou, J. Kong, E. Yenilmez, and H. Dai, Science **290**, 1552 (2000).

[20] J. Hone, B. Batlogg, Z. Benes, A.T. Johson, and J.E. Fischer, Science **289**, 1730 (2000); M. Freitag, M. Radosavljevic, Y. Zhou, A.T. Johnson and W.F. Smith, Appl. Phys. Lett. **79**, 3326 (2001).

[21] M. S. Gudiksen, L. J. Lauhon, J. Wang, D. Smith, and C. M. Lieber, Nature **415**, 617 (2002); Y. Xia, P. Yang, Y. Sun, Y. Wu, B. Mayers, B. Gates, Y. Yin, F. Kim, and H. Yan, Adv. Mater. **15**, 353 (2003).

[22] Y. Xue and S. Datta, Phys. Rev. Lett. 83, 4844 (1999); Y. Xue and S. Datta, in *Science and Applications of Nanotubes*, edited by D. Tománek and R. Enbody (Kluwer, New York, 2000).

[23] F. Leónard and J. Tersoff, Phys. Rev. Lett. **83**, 5174 (1999); **84**, 4693 (2000).

[24] A.A. Odintsov, Phys. Rev. Lett. 85, 150 (2000).

[25] C.L. Kane and E.J. Mele, Appl. Phys. Lett. **78**, 114 (2001).

[26] T. Nakanishi, A. Bachtold and C. Dekker, Phys. Rev. B **66**, 73307 (2002).

[27] E.H. Rhoderick and R.H. Williams, *Metal-Semiconductor Contacts*, 2nd edition (Clarendon Press, Oxford, 1988); H.K. Henisch, *Semiconductor Contacts* (Clarendon Press, Oxford, 1984).

[28] P.-W. Chiu, M. Kaempgen, and S. Roth, Phys. Rev. Lett. **92**, 246802 (2004); G. Chen, S. Bandow, E.R. Margine, C. Nisoli, A.N. Kolmogorov, V.H. Crespi, R. Gupta, G.U. Sumanasekera, S. Iijima, and P.C. Eklund, *ibid.* **90**, 257403 (2003).

[29] E. D. Minot, Y. Yaish, V. Sazonova, J.-Y. Park, M. Brink, and P.L. McEuen, Phys. Rev. Lett. **90**, 156401 (2003); J. Cao, Q. Wang, and H. Dai, *ibid.* **90**, 157601 (2003).

[30] V. Derycke, R. Martel, J. Appenzeller and Ph. Avouris, Appl. Phys. Lett. **80**, 2773 (2002); S. Heinze, J. Tersoff, R. Martel, V. Derycke, J. Appenzeller, and Ph. Avouris, Phys. Rev. Lett. **89**, 106801 (2002); S.J. Wind, J. Appenzeller, and Ph. Avouris, *ibid.* **91**, 58301 (2003).

[31] A. Javey, J. Guo, Q. Wang, M. Lundstrom, and H. Dai, Nature **424**, 654 (2003); J. Tersoff, *ibid.* **424**, 622 (2003).

[32] Y. Yaish, J.-Y. Park, S. Rosenblatt, V. Sazonova, M. Brink, and P.L. McEuen, Phys. Rev. Lett. **92**, 46401 (2004).

[33] W. Mönch, Rep. Prog. Phys. **53**, 221 (1990); See also W. Mönch, *Semiconductor surfaces and interfaces*, 2nd edition (Springer, Berlin, 1995).

[34] G. Margaritondo, Rep. Prog. Phys. **62**, 765 (1999); M. Peressi, N. Binggeli, and A. Baldereschi, J. Phys. D **31**, 1273 (1998).

[35] W. Mönch, J. Vac. Sci. Technol. B **17**, 1867 (1999); R.T. Tung, Phys. Rev. Lett. **84**, 6078 (2000).

[36] F. Berz, Solid-State Electron. **28**, 1007 (1985); C.M. Maziar and M.S. Lundstrom, Electron. Lett. **23**, 61 (1987).

[37] R. Landauer, Physica Scripta **T42**, 110 (1992); J. Phys.: Condens. Matter **1**, 8099 (1989).

[38] T. Ando and T. Nakanishi, J. Phys. Soc. Jpn. **67**, 1704 (1998); T. Ando, T. Nakanishi, and R. Saito, *ibid.* **67**, 2857 (1998).

[39] C.L. Kane and E.J. Mele, Phys. Rev. Lett. **78**, 1932 (1997); Z. Yao, C.L. Kane, and C. Dekker, *ibid.* **84**, 2941 (2000).

[40] C.T. White and T.N. Todorov, Nature **393**, 240 (1998).

[41] J.-Y. Park, S. Rosenblatt, Y. Yaish, V.Sazonova, H. Ustunel, S. Braig, T. A. Arias, P. Brouwer and P.L. McEuen, Nano Lett. **4**, 517 (2004); A. Javey, J. Guo, M. Paulsson, Q. Wang, D. Mann, M. Lundstrom and H. Dai, Phys. Rev. Lett. **92**, 106804 (2004).

[42] R.W. Keyes, Proc. IEEE **89**, 227 (2001); **63**, 740 (1975).

[43] J. Guo, S. Datta, M. Lundstrom, M. Brink, P. McEuen, A. Javey, H. Dai, H. Kim, and P. McIntyre, in *IEDM Tech. Dig.*, Dec. 2002, p. 29.3.

[44] D. Orlikowski, H. Mehrez, J. Taylor, H. Guo, J. Wang, and C. Roland, Phys. Rev. B **63**, 155412 (2001).

[45] Y. Xue and M.A. Ratner, Appl. Phys. Lett. **83**, 2429 (2003).

[46] Y. Xue and M.A. Ratner, Phys. Rev. B. **69**, 161402(R) (2004).

[47] S. Dag, O. Gülseren, S. Ciraci, and T. Yildirim, Appl. Phys. Lett. **83**, 3180 (2003).
[48] For recent reviews, see M.A. Reed, Proc. IEEE **97**, 652 (1999); C. Joachim, J.K. Gimzewski and A. Aviram, Nature **408**, 541 (2000); A. Nitzan and M.A. Ratner, Science **300**, 1384 (2003); J.R. Heath and M.A. Ratner, Phys. Today **56**(5), 43 (2003) and references thererein.
[49] Y. Xue, S. Datta and M. A. Ratner, J. Chem. Phys. **115**, 4292 (2001).
[50] Y. Xue and M.A. Ratner, Phys. Rev. B **68**, 115406 (2003); **68**, 115407 (2003); **69**, 85403 (2004).
[51] C.W.J. Beenakker and H. van Houten, Solid State Phys. **44**, 1 (1991); Y. Imry and R. Landauer, Rev. Mod. Phys. **71**, S306 (1999); Y. Imry, *Introduction to Mesoscopic Physics*, 2nd edition (Oxford University Press, Oxford, 2002).
[52] M. Büttiker, Phys. Rev. Lett. 57, 1761-1764 (1986).
[53] R. Landauer, IBM J. Res. Develop. **32**, 306 (1988); M. Büttiker, *ibid.* **32**, 317 (1988).
[54] Y. Xue, S. Datta and M. A. Ratner, J. Chem. Phys. **115**, 4292 (2001); Chem. Phys. **281**, 151 (2002); Y. Xue, Ph.D. thesis, School of Electrical and Computer Engineering, Purdue University (2000).
[55] J. Taylor, H. Guo, and J. Wang, Phys. Rev. B **63**, 245407 (2001); C.-C. Kaun, B. Larade, H. Mehrez, J. Taylor, and H. Guo, Phys. Rev. B **65**, 205416 (2002).
[56] S. Datta, *Electron Transport in Mesoscopic Systems* (Cambridge University Press, Cambridge, 1995); D.K. Ferry and S.M. Goodnick, *Transport in Nanostructures* (Cambridge University Press, Cambridge, 1997).
[57] Y. Meir and N. S. Wingreen, Phys. Rev. Lett. **68**, 2512 (1992); A.P. Jauho, N.S. Wingreen and Y. Meir, Phys. Rev. B **50**, 5528 (1994); H. Haug and A-P. Jauho, *Quantum Kinetics in Transport and Optics of Semiconductors* (Springer-Verlag, Berlin, 1996).
[58] *Theory of The Inhomogeneous Electron Gas*, edited by S. Lundqvist and N.H. March (Plenum Press, New York, 1983); R.M. Dreizler and E.K.U. Gross, *Density Functional Theory: An Approach to the Quantum Many-Body Problem* (Springer-Verlag, Berlin, 1990).
[59] C. M. Goringe, D. R. Bowler and E. Hernández, Rep. Prog. Phys. **60**, 1447 (1997).
[60] R. Lake, G. Klimeck, R. C. Bowen and D. Jovanovic, J. Appl. Phys. **81**, 7845 (1997).
[61] Y. Xue, S. Datta, S. Hong, R. Reifenberger, J.I. Henderson, and C.P. Kubiak, Phys. Rev. B **59**, 7852 (1999).
[62] C. Joachim and J.F. Vinuesa, Europhys. Lett. **33**, 635 (1996); M. Magoga and C. Joachim, Phys. Rev. B **59**, 16011 (1999).
[63] W. Tian, S. Datta, S. Hong, R. Reifenberger, J.J. Henderson and C.P. Kubiak, J. Chem. Phys. **109**, 2874 (1998).
[64] V. Mujica, A.E. Roitberg, and M.A. Ratner, J. Chem. Phys. **112**, 6834 (2000).
[65] M. Elstner, D. Porezag, G. Jungnickel, J. Elsner, M. Haugk, T. Frauenheim, S. Suhai and G. Seifert, Phys. Rev. B **58**, 7260 (1998); T. Frauenheim, G. Seifert, M. Elstner, T. Niehaus, C. Köhler,M. Amkreutz, M. Sternberg, Z. Hajnal, A.D. Carlo, and S. Suhai, J. Phys.: Condens. Matter **14**, 3015 (2002).
[66] Y. Xue and M.A. Ratner, Mater. Res. Soc. Symp. Proc. **734**, B6.8 (2003).
[67] J.D. Jackson, *Classical Electrodynamics*, 2nd edition (Wiley, New York, 1975).
[68] The image plane is chosen to lie at the second atomic layer under the metal surface to avoid the divergence very close to the surface, as suggested by Lang and Kohn in their classical treatment of metal surfaces. See N.D. Lang and W. Kohn, Phys. Rev. B **1**, 4555 (1970); *ibid.* **7**, 3541 (1973).
[69] A. R. Williams, P. J. Feibelman and N. D. Lang, Phys. Rev. B **26**, 5433 (1982); R. Zeller, J. Deuta and P. H. Dederichs, Solid State Commun. **44**, 993 (1982).
[70] The work functions of gold and titanium used here are those of polycrystalline materials since the metallic electrodes used in most experiments are almost never close to being single-crystalline.
[71] *CRC Handbook of Chemistry and Physics* (CRC Press, Boca Raton, 1994).
[72] R. Hoffmann, Rev. Mod. Phys. **60**, 601 (1988) and references thererein.
[73] It has been shown by A. Rochefort, D.R. Salahub, and Ph. Avouris (J. Phys. Chem. B **103**, 641 (1999)) that EHT gives a good description of SWNT band structure as compared to the local-density-functional theory with similar minimal valence basis sets.
[74] D. A. Papaconstantopoulos, *Handbook of the Band Structure of Elemental Solids* (Plenum Press, New York, 1986).
[75] D.J. Chadi and M.L. Cohen, Phys. Stat. Sol. (b) **68**, 405 (1975).
[76] J. Tersoff and W.A. Harrison, Phys. Rev. Lett. **58**, 2367 (1987); I. Lefebvre, M. Lannoo, C. Priester, G. Allan, and C. Delerue, Phys. Rev. B **36**, 1336 (1987).
[77] J. Tersoff, Phys. Rev. Lett. **52**, 465 (1984); J. Tersoff, in *Heterojunction Band Structure Discontinuities: Physics and Device Applications*, edited by F. Capasso and G. Margaritondo (North-Holland, Amsterdam, 1987).
[78] J. Friedel, Phil. Mag. **43**, 153 (1952).
[79] J. Bardeen, Phys. Rev. **71**, 717 (1947); V. Heine, Phys. Rev. **138**, A1689 (1965); C. Tejedor, F. Flores, and E. Louis, J. Phys. C **10**, 2163 (1977).
[80] S.G. Louie and M.L. Cohen, Phys. Rev. B **13**, 2461 (1976); S.G. Louie, J.R. Chelikowsky, and M.L. Cohen, *ibid.* **15**, 2154 (1977).
[81] N.D. Lang and Ph. Avouris, Phys. Rev. Lett. **84**, 358 (2000).
[82] Note that for the metal-SWNT distance of $\Delta L = 2.5(\AA)$, there is a small difference between the calculated transfered charge and potential change reported here and those in Ref. 45 because we use a refined integration grid here. None of the conclusions reached there is affected by this difference, which also provides a numerical test for the SCTB model.
[83] F. Leónard and J. Tersoff, Appl. Phys. Lett. **81**, 4835 (2002).
[84] M. Magoga and C. Joachim, Phys. Rev. B **57**, 1820 (1998).
[85] J.K. Tomfohr and O.F. Sankey, Phys. Rev. B **65**, 245105 (2002). Although this paper was intended for devices based on short organic molecules, it is more appropriate for the SWNT junctions considered here, which are composed of repeating

units. See also G. Fagas and A. Kambili, cond-mat/0403694.
[86] C.R. Crowell and S.M. Sze, Solid-St. Electron. **9**, 1035 (1966); F.A. Padovani and R. Stratton, *ibid.* **9**, 695 (1966); K. Shenai and R.W. Dutton, IEEE Trans. Electron Devices **35**, 468 (1988).
[87] L.D. Landau and E.M. Lifshitz, *Quantum Mechanics: Non-Relativistic Theory* (Pergamon Press, Oxford, 1977).
[88] M. Büttiker, IBM J. Res. Develop. **32**, 63 (1988).
[89] M. Büttiker, J. Phys.: Condens. Matter **5**, 9361 (1993); T. Christen and M. Büttiker, Europhys. Lett. **35**, 523 (1996).
[90] E.H. Nicollian and J.R. Brews, *MOS (Metal Oxide Semiconductor) Physics and Technology* (Wiley, New York, 1982).